12-13-2002

# Efficient Reliability Estimation Approach for Analysis and Optimization of Composite Structures

Mukti Nath Singh

# EFFICIENT RELIABILITY ESTIMATION APPROACH FOR ANALYSIS AND OPTIMIZATION OF COMPOSITE STRUCTURES

By

Mukti Nath Singh

A Thesis
Submitted to the Faculty of
Mississippi State University
in Partial Fulfillment of the Requirements
for the Degree of Master of Science
in Engineering Mechanics
in the Department of Aerospace Engineering

Mississippi State, Mississippi

December 2002

EFFICIENT RELIABILITY ESTIMATION APPROACH FOR ANALYSIS AND OPTIMIZATION OF COMPOSITE STRUCTURES

By

Mukti Nath Singh

Approved:

| | |
|---|---|
| Masoud Rais-Rohani<br>Professor of Aerospace Engineering<br>(Director of Thesis) | James C. Newman, III<br>Associate Professor of Aerospace Engineering<br>(Committee Member) |
| Christopher D. Eamon<br>Assistant Professor of Civil Engineering<br>(Committee Member) | Boyd Gatlin<br>Interim Head, Department of Aerospace Engineering<br>(Graduate Coordinator) |
| A. Wayne Bennett<br>Dean of the College of Engineering | |

Name: Mukti Nath Singh

Date of Degree: December 13, 2002

Institution: Mississippi State University

Major Field: Engineering Mechanics

Major Professor: Dr. Masoud Rais-Rohani

Title of Study: EFFICIENT RELIABILITY ESTIMATION APPROACH FOR ANALYSIS AND OPTIMIZATION OF COMPOSITE STRUCTURES

Pages in Study: 61

Candidate for Degree of Master of Science

The efficient evaluation of reliability index is of considerable importance in the assessment of component reliability and reliability-based structural optimization. In this thesis, the structural reliabiltiy analysis is performed using the random sampling techniques such as traditional Monte Carlo simulation and the analytical techniques such as first-order reliability method. The feasibility of Gauss quadrature points as means of target sampling of design space and generating accurate first- and second-order response surface models of failure functions is examined. Parametric uncertainty is considered by probabilistic modeling of design parameters. Various alternative approaches for estimation of component reliability index are examined with application to two structural problems: ply failure in a multidirectional composite laminate and axial buckling of a composite circular cylinder. The probabilistic sensitivity analysis is performed to measure the influence of each random variable on the estimated reliability index. The advantages and disadvantages of each approach are discussed and the approach considered the most efficient in terms of accuracy and computational requirements is identified. Furthermore, the most efficient approach is applied in reliability-based

structural optimization of a composite circular cylinder with ply failure and axial buckling constraints. The optimization problem is solved using sequential quadratic programming based on sequential local response surface approximations of failure functions. The optimization results are presented for different geometric properties, laminate configurations, and coefficients of variation.

# ACKNOWLEDGMENTS

Truly sincere appreciation is extended to Dr. Masoud Rais-Rohani for serving as a major professor and thesis director, and for his timeless encouragement during the progress in the research. This thesis would not have been possible without providing his guidance and support which I greatly needed during the research. I would like to thank Dr. James C. Newman, III, Aerospace Engineering and Dr. Christopher D. Eamon, Civil Engineering for their valuable suggestions and comments.

My sincere thank go to Dr. Patrick Gerard of Department of Mathematics and Statistics in clarifying my doubts in writing codes in SAS. He was very helpful and prompt in replying my e-mails during crucial time of my research work. I am thankful to the Department of Aerospace Engineering for providing computer facilities, and Honda and Barrier graduate fellowship for providing financial support.

It can never be concluded without mentioning of my parents, to whom I owe every single step taken in my life. I would like to thank Vandana for always being supportive and concerned about me during the research work. Last, but not the least, I would also like to thank my colleagues, specially Satish and Thomas (my apartment mates), Raj (my room mate) and Nitin, who helped me to make this thesis in its present shape.

TABLE OF CONTENTS

LIST OF TABLES

TABLE Page

LIST OF FIGURES

# CHAPTER I

# INTRODUCTION

## 1.1 Review of Literature on Reliability Estimation

The structural reliability of a component or a system can be assessed mainly by two existing techniques in the literature: random sampling methods and analytical methods. The group of random sampling methods are dominated by traditional Monte Carlo simulation (MCS) and its variants such as stratified sampling, importance sampling and adaptive importance sampling. Torng, et. al [1] proposed a robust importance sampling method (RISM) to evaluate the probability of failure. RISM first uses a tracking scheme to locate the failure domain, and then an efficient adaptive sampling scheme is used to calculate the reliability with minimum computational effort. Bucher [2] has suggested an iterative MCS procedure utilizing results from simulation to adjust the importance sampling density. This method is mainly suitable for system reliability analysis since multiple failure modes need not be treated separately. His method reduces the statistical error of the estimated failure probability. The adaptive importance sampling (AIS) method developed by Wu [3] uses a sampling density proportional to the joint probability density function of the random variables. Using an example of a turbine blade reliability analysis, it was demonstrated that the AIS method can be used to compute system reliability and reliability sensitivities efficiently.

Analytical techniques include the first- and second-order reliability methods (FORM and SORM) that rely on the formulation of the limit-state or failure function defining the surface separating the failure and safe regions of the design space. Hasofer and

Lind [4] proposed a procedure in FORM to calculate the most probable (failure) point on the limit-state surface that was later expanded by Rackwitz and Fiessler [5] for non-normal random variables. Miki, et. al [6] developed a fundamental approach to evaluate the reliability of unidirectional fibrous composite plates under any plane stress condition. Effects of mean value, strength distribution, variation of stress, fiber orientation angle, and correlations among strengths and among applied stresses on reliability of composite plate are discussed. They show that the reliability of composite plate decreases and the fiber orientation angle that gives a maximum reliability changes with the increase in the variation of the applied stress under plane stress condition. Comparison between first-order second moment (FOSM) method and advanced first-order second moment (AFOSM) method for reliability of composite plates under plane stress condition is given. It was shown that FOSM method gives an overestimated reliability and sometimes introduces erroneous results about the orientation of maximum reliability, and so AFOSM was used to obtain a more accurate result.

Depending on the complexity of failure function evaluation, both random sampling methods and analytical methods can be extremely time consuming. This is why approximation techniques such as response surface methodology (RSM) are used to enhance the computational efficiency of structural reliability calculations. In RSM, the exact analysis procedure is modeled by an algebraic polynomial whereby the response of interest is related to the independent parameters that influence it. The unknown coefficients in the response surface (RS) model are found using a curve fitting technique such as the least squares estimation based on a pool of response samples.

Bucher and Bourgund [7] have suggested a new adaptive interpolation scheme, which enables a fast and efficient representation of the system behavior by an RS approach for structural reliability problems. The RS approach utilizes elementary statistical information, i.e., mean values and standard deviations of the basic random variables to increase the efficiency and accuracy of reliability estimation. Thus, the RS obtained

is independent of the type of distribution or correlations among the basic random variables, which enables sensitivity studies with respect to these parameters without much computational effort. It has been shown by applying RSM to various types of problems that this method is very efficient with respect to both computational effort and accuracy. It is noted that the RS does not represent the physical model exactly, but if the approximation of the physical model is selected carefully using additional stochastic information, the results of the final reliability analysis are found to be very close to the exact results. Liu and Moses [8] used a sequential RS method together with Monte Carlo importance sampling to calculate the desired reliability index.

Millwater and Wu [9] proposed a global/local method to reduce the computational requirements of probabilistic structural analysis. A coarser global model is used for most of the computations with a more refined local method used only at key probabilistic conditions. The global model is used to establish the cumulative distribution function (CDF) and the most probable point (MPP), and then the local model is used to adjust the CDF value using the predicted MPP. Shao and Murotsu [10] have developed an approximate limit-state function by using a neural network. An *active learning algorithm* is proposed to enable the network to determine important failure region by itself and also to do further learning at those regions to achieve a good fitness with the real structural state there. Rais-Rohani and Singh [11] have compared various alternative strategies for the calculation of component reliability index with application to two structural components made of composite materials. The advantages and disadvantages of each strategy are identified and the approach considered the most efficient in terms of computational requirements and accuracy is identified.

### 1.2 Review of Literature on Reliability-Based Optimization

The response surface methodology is also used extensively in structural design optimization. In a reliability-based structural optimization problem, the objective

function depends on random variables, and the design constraints include limits on minimum reliability associated with each failure mode of the structure. Liaw and DeVries [12] proposed a reliability-based optimal design process by integrating reliability and variability analysis with the optimization design process using the response surface approach. Wang, et. al [13] optimized frame and plate structures under the reliability constraint by multipoint split approximations to approximate the reliability constraint. Torng and Yang [14] optimized a structure by approximating the reliability constraint linearly and then using an advanced reliability-based optimization technique. Hendawi and Frangopol [15] proposed an optimization technique for the design of both unstiffened and stiffened hybrid composite plate girders for highway bridges.

Yang and Ma [16] developed a two-level optimum design methodology based on reliability of a composite structural system. The structural weight is taken as the objective function and the system reliability is taken as the constraint in system level optimization, while laminate reliability is taken as the objective function and weight or thickness of the laminate is taken as constraint in member level optimization. Nikolaidis and Burdisso [17] optimized a simplified aircraft wing model for system reliability using the concept of Hasofer and Lind to approximate the limit-state function about the most probable point (MPP). Tu, et. al [18] presented a new approach called performance measure approach (PMA) in the reliability-based design optimization, and they found that the conventional reliability index approach (RIA) and PMA are consistent in prescribing the probabilistic concept. They observed that PMA is inherently robust and more efficient in evaluating inactive probabilistic constraints, while RIA is more efficient for violated probabilistic constraints. Su, et. al [19] have discussed the problem of reliability-based optimization of laminated circular cylindrical shells under axial buckling instability. To improve the efficiency of both reliability analysis and design optimization, response surface methodology was used to formulate algebraic functions that relate the axial buckling of the cylindrical shell to the material and geometric random variables

that affect it. They also compared the accuracy and efficiency of the optimization results based on the sequential local response surface technique and the global response surface technique.

## 1.3 Scope of Present Work

The research work presented in this thesis is focused on development and application of a methodology that combines an analytical structural reliability technique with response surface methodology for efficient estimation of component reliability index. This work includes the use of Gauss quadrature points, associated with numerical integration of multivariable functions, in design of random experiments to obtain the data needed for estimation of unknown coefficients in selected response surface models. It also examines alternative approaches for estimation of component reliability index, and investigates the effects of parametric and modeling uncertainties through evaluation of pertinent probabilistic sensitivity derivatives in two example problems, one on first ply failure of a multidirectional composite laminate and another on axial buckling of a thin-walled composite cylinder. The developed methodology is also applied in reliability-based design optimization of a composite cylinder with buckling and ply failure constraints.

This thesis has been organized into five chapters. Following an introduction in Chapter I, Chapter II presents the basic concept behind reliability estimation and highlights various techniques to calculate reliability index followed by response surface methodology and reliability sensitivity analysis. Chapter III describes alternative approaches to estimate the reliability index, and examines their accuracy by analyzing two example problems. The most influential random variables in each case are identified by performing sensitivity analysis. Chapter IV applies the most efficient technique for reliability index estimation to solve the reliability-based structural design optimization problem. The summary and conclusions of the present work are given in Chapter V followed by appendices A through D and the list of references.

# CHAPTER II

# COMPONENT RELIABILITY ESTIMATION

## 2.1 Structural Reliability Analysis

The probability of failure of a structural component is expressed mathematically as

$$P_f = P(g(\mathbf{X}) \leq 0) \tag{2.1}$$

where $\mathbf{X} = \{X_1, X_2, ..., X_n\}^T$ is the vector of $n$ random variables and $g(\mathbf{X})$ is the limit-state (failure) function such that $g < 0$ represents failure, $g > 0$ represents safety, and $g = 0$ represents the limit-state surface separating the failure and safe regions. The probability of failure in equation (2.1) is calculated by performing the following integration:

$$P_f = \int \int ... \int_{\Omega} f_X(x_1, x_2, ..., x_n) dx_1 dx_2 ... dx_n \tag{2.2}$$

where $f_X(\mathbf{x})$ is the joint probability density function of $n$ random variables and $\Omega$ is the failure region defined by $g \leq 0$. Since the exact solution of equation (2.2) is very difficult or nearly impossible for many practical problems, several techniques have been developed to estimate $P_f$ with reasonable accuracy and computational efficiency. In the literature, $P_f$ has been estimated using a variety of random sampling techniques such as direct Monte Carlo simulation (MCS) or analytical techniques such as first- or second-order reliability method (FORM, SORM).

### 2.1.1 Monte Carlo Simulation (MCS)

In Monte Carlo simulation, $N$ independent random experiments are conducted such that the values of primary variables in each experiment are chosen in random based on the statistical properties of each variable. By conducting multiple simulation cycles, the failure probability $P_f$ and its corresponding coefficient of variation $COV(P_f)$ are calculated as

$$P_f = \frac{N_f}{N} \tag{2.3}$$

$$COV(P_f) = \frac{\sqrt{\frac{(1-P_f)P_f}{N}}}{P_f} \tag{2.4}$$

where $N_f$ is the number of simulation cycles resulting in failure ($g \leq 0$). The values of $P_f$ and $COV(P_f)$ converge to the exact values as $N$ approaches a very large number.

A random number generator is commonly used to obtain the random values based on mean, standard deviation, and distribution type of each random variable. An equation to generate random values with a normal distribution is given as [20]

$$\begin{aligned} x_1 &= \left[\sqrt{-2lnr_1}\cos(2\pi r_2)\right]\sigma_X + \mu_X \\ x_2 &= \left[\sqrt{-2lnr_1}\sin(2\pi r_2)\right]\sigma_X + \mu_X \end{aligned} \tag{2.5}$$

The two normally distributed random numbers $x_1, x_2$ with a mean $\mu_X$ and standard deviation $\sigma_X$ are generated for the given two uniformly distributed random numbers $r_1$ and $r_2$ ($0.0 \leq r_1, r_2 < 1.0$) by using equation (2.5). The two uniform random numbers $r_1$ and $r_2$ are obtained by using the Fortran library routine $r = RAN(I)$, where I is a large odd integer used as an input and $r$ is a real number obtained as an output. Each call to $RAN$ returns the next random number in the sequence. The random values for the basic random variables are generated for a given mean $\mu_X$ and a standard deviation $\sigma_X$ by using the technique described. Then, the limit-state function $g(\mathbf{X})$ is evaluated for each simulation cycle.

### 2.1.2 First-Order Reliability Method (FORM)

Although MCS gives a very convenient method to calculate the failure probability, it could be extremely time consuming to implement because of the very large number of simulation cycles required to reach convergence and obtain correct $P_f$. Analytical techniques such as FORM offer a more efficient alternative to MCS where the focus is mainly on the calculation of reliability or safety index $\beta$. In FORM, the limit-state function at the point of interest is approximated by a first-order Taylor series expansion about that point. This creates a tangent hyperplane to the limit-state function at the point of interest. The limit-state function is transformed from $x-$space (original coordinate system) to $u-$space (reduced coordinate system) in order to find the most probable point (MPP), which represents the point on limit-state surface with the highest joint probability of failure. The distance from the origin of reduced coordinate system to MPP represents $\beta$.

The mapping of general, non-normal random variables from $x-$space to $u-$space is done by matching the corresponding cumulative distribution functions at MPP (i.e., $F_{X_i}(x_i^*) = \Phi(u_i^*)$) where $F_{X_i}$ represents the cumulative distribution function (CDF) of random variable $X_i$ evaluated at MPP and $\Phi$ is the CDF of the corresponding standard normal variable $u$. In this case $u_i^*$ is defined as

$$u_i^* = \frac{x_i^* - \mu_{X_i}^N}{\sigma_{X_i}^N}, \quad i = 1, 2, ..., n \tag{2.6}$$

where $\mu_{X_i}^N$ and $\sigma_{X_i}^N$ represent the mean and standard deviation of an equivalent normal random variable, respectively, such that [5]

$$\mu_{X_i}^N = x_i^* - \sigma_{X_i}^N \Phi^{-1}\left[F_{X_i}(x_i^*)\right] \tag{2.7}$$

$$\sigma_{X_i}^N = \frac{\phi\left\{\Phi^{-1}\left[F_{X_i}(x_i^*)\right]\right\}}{f_{X_i}(x_i^*)} \tag{2.8}$$

where $F_{X_i}$ and $f_{X_i}$ represent the CDF and probability density function (PDF) of a general (non-normal) random variable $X_i$, and $\Phi$ and $\phi$ are the CDF and PDF of standard normal variate, respectively.

Reliability index $\beta$ is found by solving the following constrained optimization problem

$$\begin{aligned} &Minimize \qquad d = \sqrt{\mathbf{u}^T.\mathbf{u}} \\ &such\ that \quad g(\mathbf{X}) = g(\mathbf{U}) = 0 \end{aligned} \tag{2.9}$$

where $d_{min} = \beta$. The solution to equation (2.9) can be found using either standard mathematical programming techniques or more tailor made techniques such as that developed by Lee [21] or Rackwitz-Fiessler [5], with the former described in Appendix A.

The relation between the probability of failure and the reliability index is given as $P_f = \Phi(-\beta)$.

## 2.2 Response Surface Methodology

The procedure to calculate $\beta$, as described in Appendix A, is quite simple in principle, but it can become computationally intensive if the limit-state function is not an explicit function of random variables. To remedy this problem, response surface methodology (RSM) is used to replace the exact but implicit limit-state with an approximate explicit function in the form of an algebraic response surface (RS) model.

An RS model represents a functional relationship between the independent variables and the response variable. Typical RS models include:

(a) First-order

$$\tilde{g}(\mathbf{X}) = a_0 + \sum_{i=1}^{n} a_i X_i \tag{2.10}$$

(b) Second-order without interaction terms

$$\tilde{g}(\mathbf{X}) = a_0 + \sum_{i=1}^{n} a_i X_i + \sum_{i=1}^{n} b_{ii} X_i X_i \tag{2.11}$$

(c) Second-order with interaction terms

$$\tilde{g}(\mathbf{X}) = a_0 + \sum_{i=1}^{n} a_i X_i + \sum_{i=1}^{n} \sum_{j=1}^{i} b_{ij} X_i X_j \tag{2.12}$$

where $a_0, a_i, b_{ii}, b_{ij}$ are the unknown regression parameters. Equations (2.10-2.12) contain $n+1$, $2n+1$, and $(n+1)(n+2)/2$ unknown regression coefficients, respectively. Regression coefficients may be evaluated using a variety of statistical techniques such as the least squares estimation based on a population of response samples. First-order RS models are commonly used when the higher-order effects are negligible, while second-order RS models are used when the non-linear terms have a significant influence on the accuracy of the model. In many problems, the interaction terms have minimal effect on the response and are usually ignored. Thus, equations (2.10) and (2.11) are used as RS models to expedite the calculation of $\beta$ in this research.

A major challenge in applying RS technique is to develop an accurate model based on a relatively small number of response samples. In the literature, the direct MCS and central composite design (CCD) scheme are often used. However, in both the cases, a very large number of response samples need to be generated. CCD scheme requires $2^n + 2n + 1$ function evaluations in order to obtain an RS model involving $n$ random variables. The method proposed by Bucher and Bourgund [7] uses adaptive importance sampling which requires $4n + 3$ evaluations of the exact limit-state function. In this study, an alternative technique is examined in order to reduce the number of response samples needed for accurate estimation of regression coefficients.

In this technique, Gauss quadrature points used for numerical integration of multivariable functions [22] are used to identify target sampling points. At each target

point, the values of random variables are specified and an exact limit-state function evaluation is performed to obtain a sample response. The population of response samples and corresponding values of random variables are used to calculate the regression coefficients in the RS model. The details of this procedure are described in Appendix B.

## 2.3 Reliability Sensitivity Analysis

The probabilistic sensitivity derivatives of $\beta$ with respect to the mean $\mu_{X_i}$ and standard deviation $\sigma_{X_i}$ of each random variable are evaluated as

$$\frac{\partial \beta}{\partial \mu_{X_i}} = -\frac{u_i^*}{\beta \sigma_{X_i}}, \quad i = 1, 2, ..., n \tag{2.13}$$

$$\frac{\partial \beta}{\partial \sigma_{X_i}} = -\frac{u_i^{*2}}{\beta \sigma_{X_i}}, \quad i = 1, 2, ..., n \tag{2.14}$$

Sensitivity factors in equation (2.13) quantify the influence of each random variable on $\beta$ while those in equation (2.14) quantify the effect of uncertainty in each random variable on $\beta$. When the random variables are of vastly different scales, it is recommended to normalize sensitivity derivatives as

$$\delta_i = \frac{\partial \beta}{\partial \mu_{X_i}} \left( \frac{\mu_{X_i}}{\beta} \right), \quad i = 1, 2, ..., n \tag{2.15}$$

$$\eta_i = \frac{\partial \beta}{\partial \sigma_{X_i}} \left( \frac{\sigma_{X_i}}{\beta} \right), \quad i = 1, 2, ..., n \tag{2.16}$$

# CHAPTER III

# APPROACHES FOR ESTIMATION OF RELIABILITY INDEX

To investigate the accuracy and computational efficiency of target sampling technique based on Gauss quadrature points, six different approaches are examined and described as follows:

Approach 1: Calculate $\beta$ directly from Monte Carlo simulation based on exact failure function evaluation at each simulation cycle. The probability of failure, $P_f$ is determined as given in equation (2.3) and then $\beta$ is found using $\beta = -\Phi^{-1}(P_f)$.

Approach 2: Calculate $\beta$ using the iterative procedure described in Appendix A. Evaluate the partial derivatives of limit-state function with respect to each random variable $(\partial g/\partial X_i)$ using forward finite-difference scheme. Find an appropriate step size parameter $\delta$ for each random variable (i.e., $\Delta X_i = \delta X_i$, here $\delta = 0.001$) that would provide reasonably accurate derivatives.

Approach 3: Calculate $\beta$ by using a first-order RS model, equation (2.10), to approximate the limit-state function. In this approach, the $n+1$ regression coefficients are obtained using $n+1$ quadrature points defined by the equation (B.2). Since the limit-state function is approximated by a first-order RS model, $\beta$ is obtained directly as

$$\beta = \frac{\mu_{\tilde{g}}}{\sigma_{\tilde{g}}} = \frac{a_0 + \sum_{i=1}^{n} a_i \mu_{X_i}}{\sqrt{\sum_{i=1}^{n} (a_i \sigma_{X_i})^2}} \tag{3.1}$$

Approach 4: Calculate $\beta$ by using a first-order RS model (as in Approach 3), but use $2n$ quadrature points defined by equation (B.4) to estimate the regression coefficients.

Approach 5: Estimate $\beta$ by using a second-order RS model (equation (2.11)) of limit-state function. In this approach, the $2n+1$ regression coefficients are obtained using $2n$ quadrature points defined by equation (B.4) and $Z_{2n+1,j} = (0, 0, ..., 0)$. Hence, $2n+1$ response samples are used to estimate the $2n+1$ regression coefficients. Then, $\beta$ is determined using the iterative procedure described in Appendix A. The difference between this approach and Approach 2 is that here the limit-state function is approximated by a second-order RS model. The derivatives of limit-state function are obtained directly from analytical differentiation of the RS model. It is also important to point out that the coefficients of the RS model are calculated only one time during the iterative process to calculate $\beta$.

Approach 6: Estimate $\beta$ similar to that described in Approach 5. However, in this approach, the derivatives of limit-state function are obtained from the second-order RS model while the exact evaluation of limit-state function for $g(\mathbf{X}^*)$ (refer Appendix A) is performed at each iteration step for $\beta$.

The computational efficiency and accuracy of the six approaches (described above) are examined in two example problems: ply failure in a multidirectional composite laminate and axial buckling of a composite circular cylinder. Laminate configuration identified for the analysis is $L1 : [\pm 45/90_4/\mp 45]_s$ with 16 plies made of carbon/epoxy (AS4 12k/3502) unidirectional tape.

### 3.1 Example 1: Ply Failure in a Multidirectional Composite Laminate

A multidirectional composite laminate in a state of plane stress with all laminae perfectly bonded together has been considered for first-ply failure (FPF) analysis. The classical lamination plate theory (CLPT) is used to obtain the in-plane stresses in principal material directions (PMD). Considering laminate symmetry and the absence of bending and twisting moments, the in-plane stresses in PMD in the $k^{th}$ ply can be

calculated as

$$\{\sigma\}_k = [T]_k \left[\bar{Q}\right]_k [A]^{-1}\{N\} \tag{3.2}$$

where $[T]_k$ and $\left[\bar{Q}\right]_k$ are the transformation and the transformed reduced stiffness matrix of $k^{th}$ layer, respectively. $[A]$ is the laminate extension stiffness matrix, $\{N\}$ is the stress resultant vector such that $\{N\}^T = \{N_x, N_y, N_{xy}\}$, and $\{\sigma\}_k^T = \{\sigma_1, \sigma_2, \tau_{12}\}_k$. The details for the calculation of the in-plane stresses in PMD in the $k^{th}$ ply are given in Appendix C.

After calculating in-plane stresses, Tsai-Wu (Interactive Tensor Polynomial) criterion is used to formulate the limit-state function for $k^{th}$ ply. Tsai-Wu failure criterion is based on the total strain energy failure theory of Beltrami with the failure boundary described in contracted notation by the equation

$$f_i\sigma_i + f_{ij}\sigma_i\sigma_j = 1, \quad i,j = 1,2,...,6 \tag{3.3}$$

where $f_i$, $f_{ij}$ are the second and fourth order strength tensors, respectively. For an orthotropic lamina in a state of plane stress, the equation above reduces to

$$f_1\sigma_1 + f_2\sigma_2 + f_{11}\sigma_1^2 + f_{22}\sigma_2^2 + f_{66}\sigma_6^2 + 2f_{12}\sigma_1\sigma_2 = 1 \tag{3.4}$$

where $\sigma_6 = \tau_{12}$. Note that $f_{16} = f_{26} = f_6 = 0$ since the shear strength in PMD is independent of the sign of shear stress. The remaining strength tensors are found as follows:

$$\begin{aligned} f_1 &= \tfrac{1}{F_1^t} - \tfrac{1}{F_1^c}; \quad & f_{11} &= \tfrac{1}{F_1^t F_1^c} \\ f_2 &= \tfrac{1}{F_2^t} - \tfrac{1}{F_2^c}; \quad & f_{22} &= \tfrac{1}{F_2^t F_2^c} \\ f_{66} &= \tfrac{1}{F_{12}^2}; & f_{12} &= -\tfrac{1}{2}\sqrt{\tfrac{1}{F_1^t F_1^c F_2^t F_2^c}} \end{aligned} \tag{3.5}$$

The limit-state function for $k^{th}$ ply is defined as

$$g^k = 1 - (f_1\sigma_1 + f_2\sigma_2 + f_{11}\sigma_1^2 + f_{22}\sigma_2^2 + f_{66}\tau_{12}^2 + 2f_{12}\sigma_1\sigma_2)_k \tag{3.6}$$

Before performing $\beta$ calculation, the FPF load has been calculated in the laminate. It has been observed based on Tsai-Wu failure theory for loading condition $\{N\}^T = \{N_x, 0, 0\}$ that the $\pm 45^0$ and $90^0$ layers are weaker and more likely to fail if the laminate is loaded in the axial tension while the $0^0$ layers are weaker and more likely to fail if the laminate is loaded in the axial compression. In the case of laminate $L1$, the $90^0$ ply group is the first to fail at a load of $N_x = 1,352\ lb/in.$ These findings are useful in finding out the weakest ply in a laminate.

### 3.1.1 Comparison of Results for Approaches 1 through 6

The statistical characteristics (mean, coefficient of variation) of the material properties affecting ply failure, obtained from MIL-HDBK-17-2E [23], are given in Table 3.1. It is assumed that all random variables are normally distributed, uncorrelated and statistically independent. The applied axial load $N_x$ is assumed deterministic. Since

Table 3.1: Statistical characteristics of random variables affecting ply failure

| Random Variable | Distribution Type | Mean Value | COV (%) |
|---|---|---|---|
| $E_1$ | Normal | 18.0e6 psi | 3.19 |
| $E_2$ | Normal | 1.35e6 psi | 4.26 |
| $\nu_{12}$ | Normal | 0.226 | 5.00 |
| $G_{12}$ | Normal | 0.543e6 psi | 5.16 |
| $F_1^t$ | Normal | 258e3 psi | 9.83 |
| $F_1^c$ | Normal | 204e3 psi | 6.45 |
| $F_2^t$ | Normal | 7.76e3 psi | 10.70 |
| $F_2^c$ | Normal | 34.6e3 psi | 9.53 |
| $F_{12}$ | Normal | 14.8e3 psi | 3.18 |
| $t_{ply}$ | Normal | 0.005 in. | 5.00 |
| $\theta_{ply}$ | Normal | $\pm 45^0$, $90^0$ | $5^a$ |

[a]Standard Deviation

the $90^0$ ply group is more likely to fail in laminate $L1$ under axial tensile load, the reliability index, $\beta$ associated with failure in this $90^0$ ply group is calculated and used for comparative study. The estimated values of $\beta$ in each approach for different values

of applied load are given in Table 3.2. For Approaches 2, 5, and 6 involving an iterative procedure for $\beta$, $|g| \leq 0.001$ and $|\beta_{m+1} - \beta_m| \leq 0.0001$ ($m$ denotes iteration number) are used as hard and soft convergence criteria, respectively.

Table 3.2: Estimated values of $\beta$ for the $90^0$ ply group for Approaches 1-6

| Nx, | Approach | | | | | |
|---|---|---|---|---|---|---|
| lb/in | 1 | 2 | 3 | 4 | 5 | 6 |
| 1200 | 0.54 | 0.60 | 0.52 | 0.48 | 0.60 | 0.60 |
| 1000 | 1.45 | 1.52 | 1.74 | 1.63 | 1.65 | 1.53 |
| 800 | 2.56 | 2.66 | 3.68 | 3.40 | 3.10 | 2.67 |
| 700 | 3.21 | 3.33 | 5.11 | 4.70 | 4.07 | 3.33 |

For Approach 1, $\beta$ calculation is based on 3000 exact evaluations of failure function in equation (3.6). For Approach 2, the number of exact failure function evaluations is $m(n+1)$ ($n$ is the number of random variables, here $n = 15$) and it requires $n+1$ function calls to calculate the partial derivatives ($\partial g / \partial U_i^*$) at each iteration. For the results presented in Table 3.2, $m = 3,\ 4,\ 5,\ 6$ for $N_x = 1200,\ 1000,\ 800,\ 700\ lb/in.$, respectively. For Approaches 3, 4, and 5, the number of exact failure function evaluation is $n+1$, $2n$, and $2n+1$ respectively. For Approach 6, the number of exact failure function evaluations is $2n+1+m$, where $m = 4,\ 8,\ 15,\ 24$ for $N_x = 1200,\ 1000,\ 800,\ 700\ lb/in.$, respectively. The total number of exact failure function evaluations for each approach and load combination is given in given in Table 3.3. Figure 3.1 depicts the graphical comparison of $\beta$ in each approach for different values of applied load.

It could be observed in Figure 3.1 that for all the approaches, $\beta$ increases as $N_x$ decreases. For Approaches 3, 4, and 5, the $\beta$ values deviate significantly compare to the Approach 1 i.e., MCS as $\beta$ increases. While, for Approaches 2 and 6, $\beta$ values agree reasonably well with those obtained from MCS at a considerably less computational cost. Comparing Approaches 1, 2, and 6, the results of Approach 2 is closer to Approach 1, but by a relatively insignificant amount. But, when considering the number of exact failure function evaluations in Table 3.3 for Approaches 1, 2, and 6, it is evident that

Table 3.3: Number of exact ply failure function evaluations for the $90^0$ ply group for Approaches 1-6

| Nx, lb/in | Approach | | | | | |
|---|---|---|---|---|---|---|
| | 1 | 2 | 3 | 4 | 5 | 6 |
| 1200 | 3000 | 48 | 16 | 30 | 31 | 35 |
| 1000 | 3000 | 64 | 16 | 30 | 31 | 39 |
| 800 | 3000 | 80 | 16 | 30 | 31 | 46 |
| 700 | 3000 | 96 | 16 | 30 | 31 | 55 |

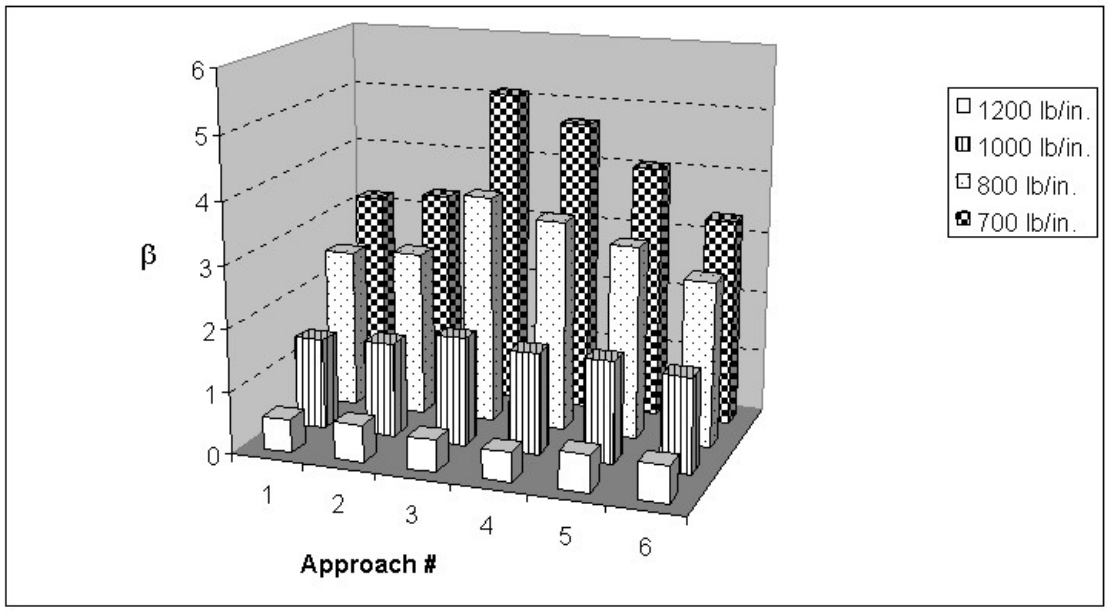


Figure 3.1: Comparison of $\beta$ for the $90^0$ ply group for Approaches 1-6

Approach 6 is overall more efficient than the other two. It could be seen from Table 3.4 that Approach 6 is more efficient even for higher COVs. Table 3.4 presents $\beta$ value and number of exact ply failure function evaluations for the $90^0$ ply group for Approaches 2 and 6 for COVs of 10% and 20% for all random variables except ply orientation angles with standard deviation kept at $5^0$. The mean value of all random variables and standard deviation of ply orientation angles are kept the same as those specified in Table 3.1.

Table 3.4: The effect of increasing COVs on $\beta$ and number of exact ply failure function evaluations for the $90^0$ ply group for Approaches 2 and 6 at $N_x = 700\ lb/in.$

| | COV=10% | | COV=20% | |
|---|---|---|---|---|
| | Approach 2 | Approach 6 | Approach 2 | Approach 6 |
| $\beta$ | 3.16 | 3.18 | 1.94 | 2.08 |
| $NFE^a$ | 80 | 44 | 80 | 37 |

[a] $NFE$ : number of exact ply failure function evaluations

The values of basic random variables at the design point or MPP for $N_x = 700\ lb/in.$ in Approaches 2 and 6 are compared in Table 3.5. The effect of increasing COVs on MPP value is shown in Table 3.6. The MPP values represent the worst combination of design properties resulting in ply failure.

Table 3.5: Comparison of mean and MPP values for the $90^0$ ply group for Approaches 2 and 6 at $N_x = 700\ lb/in.$

| Random Variable | Mean Value | MPP Value | |
|---|---|---|---|
| | | Approach 2 | Approach 6 |
| $E_1, E+06\ psi$ | 18.0 | 17.89 | 17.88 |
| $E_2, E+06\ psi$ | 1.35 | 1.371 | 1.370 |
| $\nu_{12}$ | 0.226 | 0.22565 | 0.22571 |
| $G_{12}, E+06\ psi$ | 0.543 | 0.539 | 0.541 |
| $F_1^t, E+03\ psi$ | 258 | 259.14 | 260.06 |
| $F_1^c, E+03\ psi$ | 204 | 203.15 | 202.86 |
| $F_2^t, E+03\ psi$ | 7.76 | 5.86 | 5.72 |
| $F_2^c, E+03\ psi$ | 34.6 | 34.58 | 35.01 |
| $F_{12}, E+03\ psi$ | 14.8 | 14.80 | 14.80 |
| $t_{45},\ in.$ | 0.02 | 0.01976 | 0.01980 |
| $t_{-45},\ in.$ | 0.02 | 0.01976 | 0.01980 |
| $t_{90},\ in.$ | 0.04 | 0.03927 | 0.03959 |
| $\theta_{45},\ deg.$ | 45 | 53.243 | 52.784 |
| $\theta_{-45},\ deg.$ | -45 | -53.243 | -52.784 |
| $\theta_{90},\ deg.$ | 90 | 90.0021 | 90.0019 |

Table 3.6: The effect of increasing COVs on MPP values for the $90^0$ ply group for Approaches 2 and 6 at $N_x = 700\ lb/in.$

| Random Variable (RV) | Mean Value | MPP Value | | | |
|---|---|---|---|---|---|
| | | $COV = 10\%$ | | $COV = 20\%$ | |
| | | Approach 2 | Approach 6 | Approach 2 | Approach 6 |
| $E_1, E+06\ psi$ | 18.0 | 16.9 | 16.6 | 16.0 | 16.7 |
| $E_2, E+06\ psi$ | 1.35 | 1.45 | 1.45 | 1.51 | 1.43 |
| $\nu_{12}$ | 0.226 | 0.22459 | 0.22487 | 0.22393 | 0.22517 |
| $G_{12}, E+06\ psi$ | 0.543 | 0.529 | 0.535 | 0.526 | 0.537 |
| $F_1^t, E+03\ psi$ | 258 | 259.09 | 260.06 | 259.39 | 261.30 |
| $F_1^c, E+03\ psi$ | 204 | 202.05 | 201.05 | 201.59 | 199.39 |
| $F_2^t, E+03\ psi$ | 7.76 | 6.31 | 6.23 | 5.55 | 4.73 |
| $F_2^c, E+03\ psi$ | 34.6 | 34.58 | 35.04 | 34.57 | 35.30 |
| $F_{12}, E+03\ psi$ | 14.8 | 14.80 | 14.80 | 14.80 | 14.80 |
| $t_{45},\ in.$ | 0.02 | 0.0191 | 0.0191 | 0.0186 | 0.0191 |
| $t_{-45},\ in.$ | 0.02 | 0.0191 | 0.0191 | 0.0186 | 0.0191 |
| $t_{90},\ in.$ | 0.04 | 0.0370 | 0.0382 | 0.0364 | 0.0380 |
| $\theta_{45},\ deg.$ | 45 | 52.461 | 52.456 | 47.730 | 46.217 |
| $\theta_{-45},\ deg.$ | -45 | -52.473 | -52.456 | -47.730 | -45.940 |
| $\theta_{90},\ deg.$ | 90 | 90.0022 | 90.0018 | 90.0002 | 90.0003 |

### 3.1.2 Sensitivity Analysis

The probabilistic sensitivity derivatives are calculated using equations (2.13) and (2.14), and are normalized using equations (2.15) and (2.16). The original and normalized derivatives for Approach 2 are shown in Table 3.7. Normalized probabilistic sensitivity derivatives of $\beta$ with respect to the mean and standard deviation of each random variable is shown in the Figure 3.2. Among all random variables affecting the ply failure, tensile failure strength $F_2^t$ is found to have the greatest influence, followed by orientation angle of the $\pm 45^0$ plies, and elastic moduli $E_2$ and $E_1$. Parametric uncertainty is represented by the normalized probabilistic sensitivity derivatives with respect to the standard deviation as shown in column 5, Table 3.7. The negative sign in column 5 indicates that as the uncertainty is reduced, $\beta$ is increased.

Table 3.7: Probabilistic sensitivity derivatives of $\beta$ for the $90^0$ ply group for Approach 2 at $N_x = 700\ lb/in$.

| RV | $\frac{\partial \beta}{\partial \mu_{X_i}}$ | $\delta_i$ | $\frac{\partial \beta}{\partial \sigma_{X_i}}$ | $\eta_i$ |
|---|---|---|---|---|
| $E_1$ | 1.01E-07 | 0.546 | -1.95E-08 | -0.0034 |
| $E_2$ | -1.92E-06 | -0.777 | -7.05E-07 | -0.0123 |
| $\nu_{12}$ | 8.29E-01 | 0.056 | -2.59E-02 | -0.0001 |
| $G_{12}$ | 1.52E-06 | 0.248 | -2.16E-07 | 0.0000 |
| $F_1^t$ | -5.43E-07 | -0.041 | -2.41E-08 | -0.0002 |
| $F_1^c$ | 1.48E-06 | 0.091 | -9.58E-08 | -0.0004 |
| $F_2^t$ | 8.25E-04 | 1.924 | -1.89E-03 | -0.4700 |
| $F_2^c$ | 6.45E-07 | 0.007 | -4.57E-09 | 0.0000 |
| $F_{12}$ | 0.00E+00 | 0.000 | 0.00E+00 | 0.0000 |
| $t_{\pm 45}$ | 7.23E+01 | 0.109 | -1.74E+01 | -0.0013 |
| $t_{90}$ | 5.50E+01 | 0.083 | -2.01E+01 | -0.0015 |
| $\theta_{\pm 45}$ | -9.90E-02 | -1.337 | -1.63E-01 | -0.2450 |
| $\theta_{90}$ | -2.53E-05 | -0.001 | -1.07E-08 | 0.0000 |

The most important normalized probabilistic sensitivity derivatives, identified in Figure 3.2, obtained for Approaches 2-6 are presented in Table 3.8 and Figure 3.3

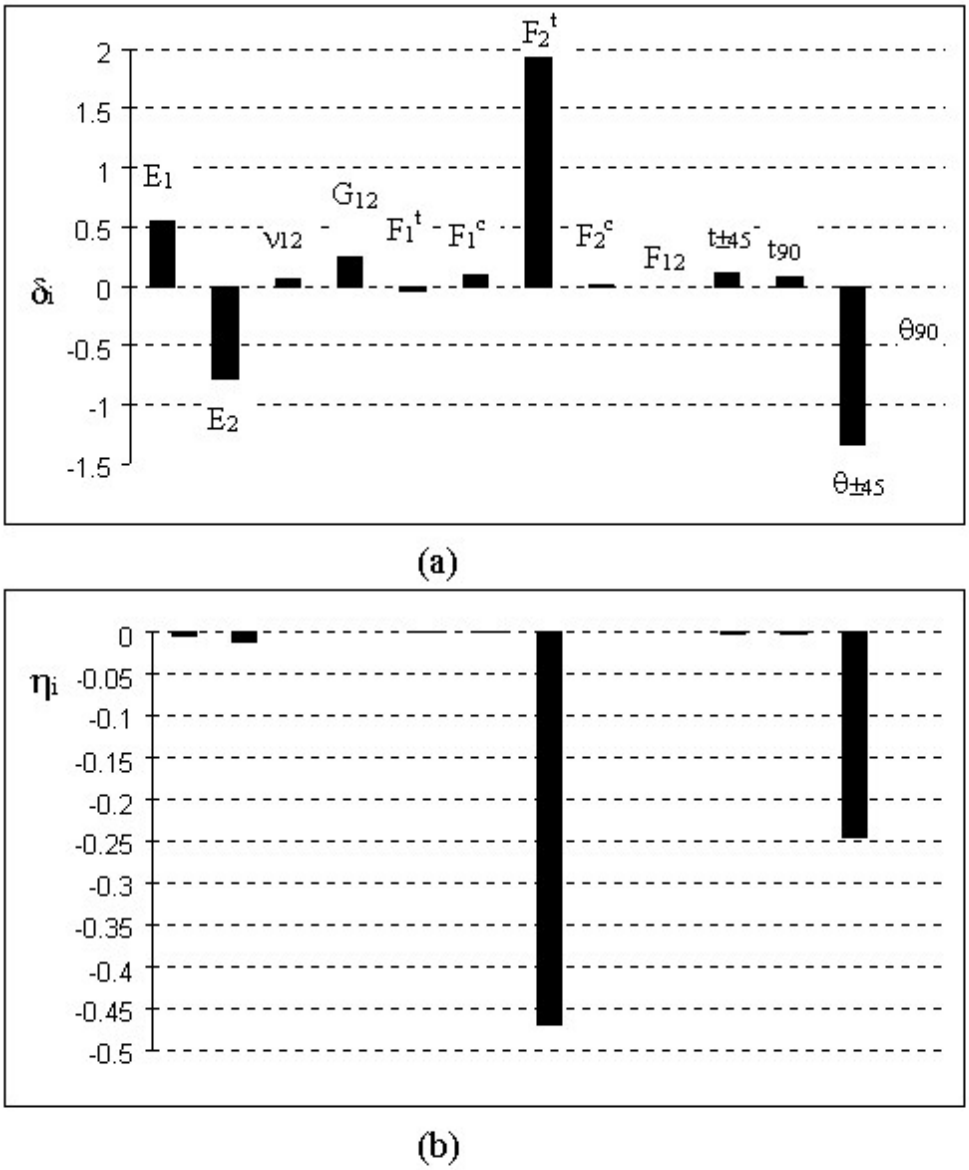


Figure 3.2: Normalized probabilistic sensitivity derivatives of $\beta$ for the $90^0$ ply group with respect to the (a) mean and (b) standard deviation of each random variable for Approach 2 at $N_x = 700\ lb/in$.

for comparison. The effect of increasing COVs on normalized probabilistic sensitivity derivatives are given in Table 3.9.

Table 3.8: Normalized probabilistic sensitivity derivatives $\delta_i$ for the $90^0$ ply group for Approaches 2-6 at $N_x = 700\ lb/in$.

| | Approach | | | | |
|---|---|---|---|---|---|
| RV | 2 | 3 | 4 | 5 | 6 |
| $E_1$ | 0.546 | 0.693 | 0.556 | 0.468 | 0.600 |
| $E_2$ | -0.777 | -0.517 | -0.684 | -0.566 | -0.728 |
| $F_2^t$ | 1.924 | 0.826 | 1.254 | 1.728 | 2.045 |
| $\theta^a_{\pm 45}$ | -1.337 | -1.206 | -1.010 | -0.998 | -1.250 |

[a] $\delta_i$ shown for Approach 3 is for $+45^0$ layer. For the $-45^0$ layer, $\delta_i$ is -0.851.

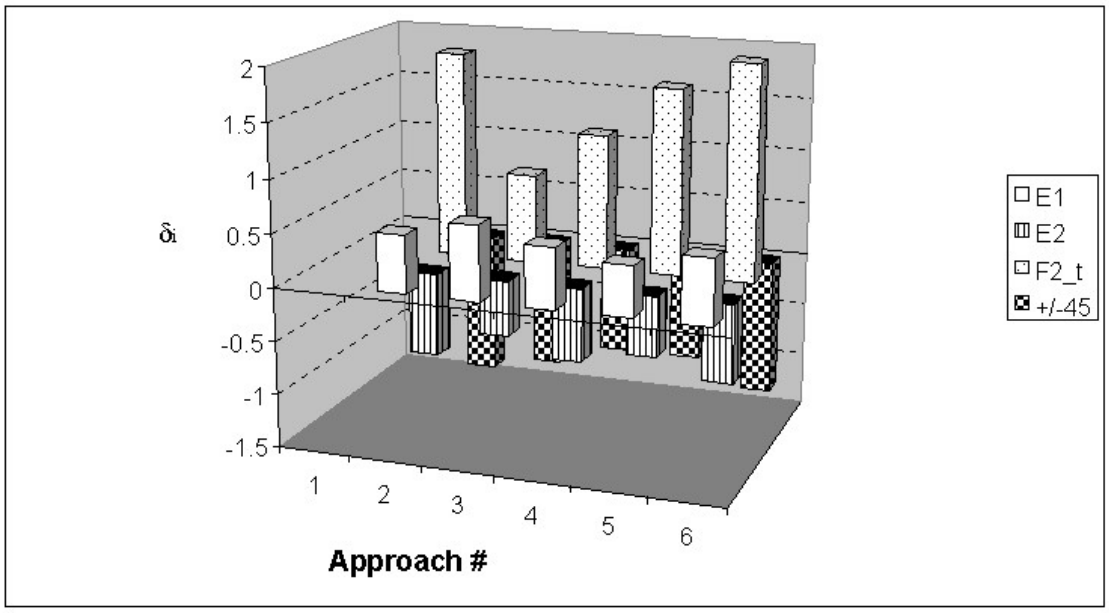


Figure 3.3: Comparison of $\delta_i$ for the $90^0$ ply group for Approaches 2-6 at $N_x = 700\ lb/in$.

It is observed in Figure 3.3 that the best overall agreement is between Approaches 2 and 6. For $E_1$ and $E_2$, the derivatives obtained from the linear RS model in Approach 4 are much closer to those in Approach 2 than those found in Approaches 3 and 5. It is important to note that even a simple linear model as in Approaches 3 and 4 is capable of

Table 3.9: The effect of increasing COVs on normalized probabilistic sensitivity derivatives for the $90^0$ ply group for Approaches 2 and 6 at $N_x = 700\ lb/in.$

| | COV=10% | | | | COV=20% | | | |
|---|---|---|---|---|---|---|---|---|
| | Approach 2 | | Approach 6 | | Approach 2 | | Approach 6 | |
| RV | $\delta_i$ | $\eta_i$ | $\delta_i$ | $\eta_i$ | $\delta_i$ | $\eta_i$ | $\delta_i$ | $\eta_i$ |
| $E_1$ | 0.605 | -0.0366 | 0.743 | -0.0559 | 0.738 | -0.0818 | 0.401 | -0.0279 |
| $E_2$ | -0.769 | -0.0591 | -0.761 | -0.0586 | -0.776 | -0.0904 | -0.333 | -0.0192 |
| $F_2^t$ | 1.87 | -0.3506 | 1.94 | -0.3823 | 1.90 | -0.5403 | 2.25 | -0.8809 |
| $\theta_{\pm 45}$ | -1.34 | -0.2229 | -1.33 | -0.2197 | -1.31 | -0.0794 | -0.505 | -0.0137 |

providing useful sensitivity information to identify the most influential random variables affecting the ply failure. Hence, it is reasonable to use a simple linear RS model based on $n + 1$ or $2n$ response samples to quickly identify the important random variables, and then use the more accurate model as in Approach 6 for subsequent reliability-based design optimization.

### 3.2 Example 2: Axial Buckling of a Composite Circular Cylinder

A thin-walled composite circular cylinder under a uniform axial compressive load and $L1$ laminate is considered in this example. The applied load acting on the cylinder is treated as uniform and deterministic, and the loaded edges are assumed perfectly clamped.

The limit-state function for axial buckling is expressed as

$$g = \frac{N_{cr}}{N_x} - 1 \tag{3.7}$$

where $N_{cr}$ is the axial buckling load obtained directly from shell analysis code [24], and $N_x$ is the deterministic applied load. The structural model of the circular cylinder is given in Figure 3.4. All boundary conditions required to simulate the computational

model of the circular cylindrical shell are specified in Table 3.10. The mathematical procedure to calculate the cylinder axial buckling load is given in Appendix D.

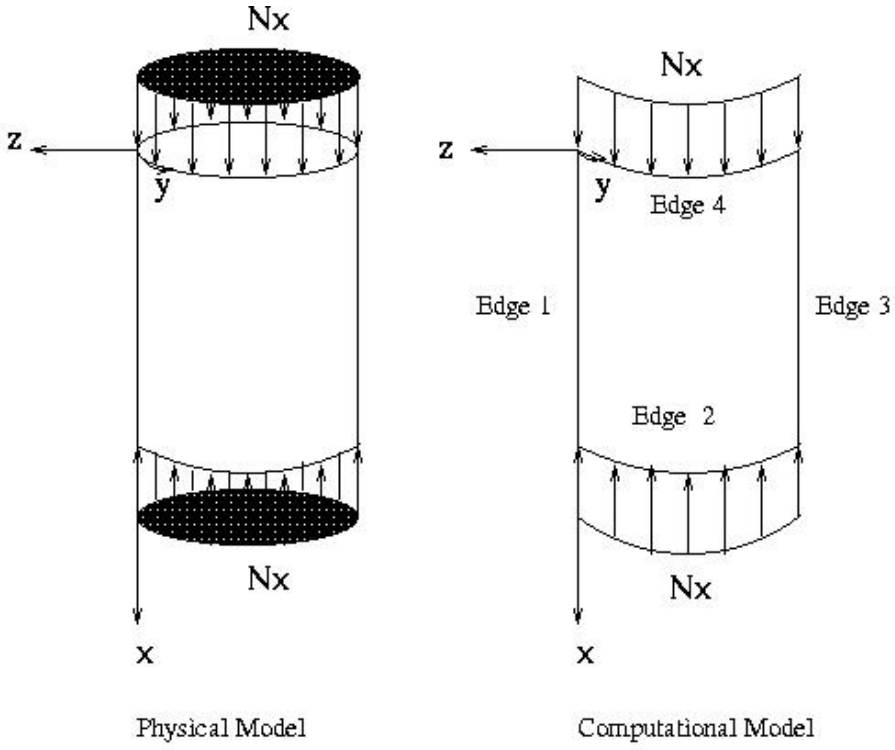


Figure 3.4: Physical and computational model of the circular cylindrical shell

Table 3.10: Description of boundary conditions for the shell model[a]

| Displacement | Edge 1 | Edge 2 | Edge 3 | Edge 4 |
|---|---|---|---|---|
| $u$ | 0 | 1 | 0 | 0 |
| $v$ | 1 | 1 | 1 | 1 |
| $w$ | 0 | 1 | 0 | 1 |
| $\phi_x$ | 0 | 1 | 0 | 1 |
| $\phi_y$ | 1 | 1 | 1 | 1 |

[a] 0=free, 1=fixed

Equation (3.7) is an implicit function of all the random variables affecting axial buckling load, similar to equation (3.6). Here, the exact calculation of limit-state function requires a rather time consuming eigenvalue analysis (equation (D.7)). Therefore, in the context of reliability-based design optimization where reliability index and derivatives of limit-state function are calculated repeatedly, computational time could pose a problem. Hence, only Approaches 2 through 6 are considered with the results compared for various applied loads.

### 3.2.1 Comparison of Results for Approaches 2 through 6

The exact buckling failure function refers to equation (3.7), and is approximated by the first- and second-order RS models defined by equations (2.10) and (2.11), respectively. The statistical characteristics of the material properties [23] affecting axial buckling are given in Table 3.11. The buckling failure function is a function of $n = 10$ uncorrelated and statistically independent random variables.

Table 3.11: Statistical characteristics of random variables affecting axial buckling

| Random Variable | Distribution Type | Mean Value | COV (%) |
|---|---|---|---|
| $E_1$ | Normal | 18.0e6 psi | 3.19 |
| $E_2$ | Normal | 1.35e6 psi | 4.26 |
| $\nu_{12}$ | Normal | 0.226 | 5.00 |
| $G_{12}$ | Normal | 0.543e6 psi | 5.16 |
| $t_{ply}$ | Normal | 0.005 in. | 5.00 |
| $\theta_{ply}$ | Normal | $\pm 45^0$, $90^0$ | $5^a$ |
| $D$ | Normal | 10 in. | 5.00 |
| $L$ | Normal | 20 in. | 5.00 |

[a] Standard Deviation

The estimated values of $\beta$ for axial buckling load from Approaches 2 through 6 are presented in Table 3.12, and $\beta$ values are compared in Figure 3.5. It is observed that the results of Approaches 2 and 6 are in fairly good agreement as compared to the rest. Approach 3 with the first-order RS model of buckling limit-state function consistently

Table 3.12: Estimated values of $\beta$ for axial buckling load in Approaches 2-6

| $N_x$, lb/in | Approach | | | | |
|---|---|---|---|---|---|
| | 2 | 3 | 4 | 5 | 6 |
| -4000 | 0.60 | 0.51 | 0.55 | 0.68 | 0.62 |
| -3500 | 1.74 | 1.61 | 1.77 | 1.87 | 1.79 |
| -3000 | 3.04 | 2.71 | 2.99 | 3.01 | 3.09 |
| -2500 | 4.58 | 3.80 | 4.21 | 4.09 | 4.75 |

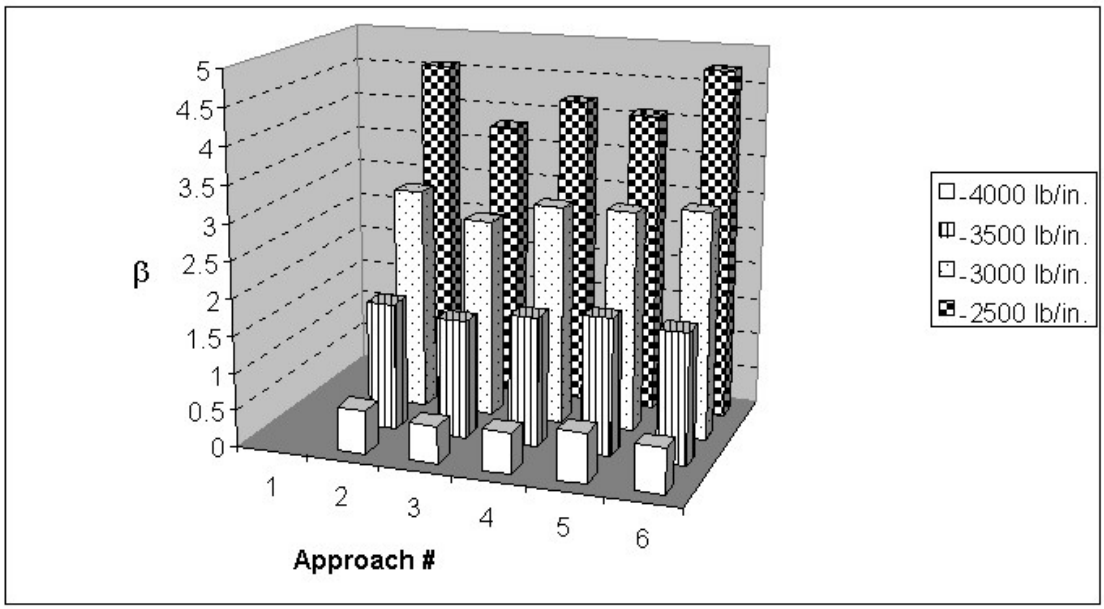


Figure 3.5: Comparison of $\beta$ for axial buckling load in Approaches 2-6

underestimates the $\beta$ value as compared to the other approaches. The results of Approach 4 with a first-oder RS model are slightly better than those in Approach 5 with a second-order RS model. In comparing Approaches 5 and 6, $\beta$ improves as a result of calculating the limit-state function exactly by calling the shell analysis code [24] at each iteration step while estimating the derivatives of limit-state function using a corresponding second-order RS model.

An indication of the computational costs for $\beta$ calculation is the number of exact failure function evaluations as given in Table 3.13. Approaches 2 and 3 are at the opposite ends of scale for computational cost with at least 33 and only 11 exact buckling failure function evaluations, respectively. The difference between Approaches 5 and 6 is not as large as that seen for ply failure. The most important comparison is again between Approaches 2 and 6. It is clearly evident that the technique used in Approach 6 is substantially more efficient than that used in Approach 2. It is seen from Table 3.14 that Approach 6 is more efficient even in presence of large scatter (i.e., higher COVs). Table 3.14 presents $\beta$ value and number of exact buckling failure function evaluations in Approaches 2 and 6 for COVs of 10% and 20% for all random variables except ply orientation angles with standard deviation kept at $5^0$. The mean value of all random variables and standard deviation of ply orientation angles are kept the same as those in Table 3.11.

Table 3.13: Number of exact buckling failure function evaluations in Approaches 2-6

| $N_x$, | Approach | | | | |
|---|---|---|---|---|---|
| lb/in | 2 | 3 | 4 | 5 | 6 |
| -4000 | 33 | 11 | 20 | 21 | 24 |
| -3500 | 33 | 11 | 20 | 21 | 25 |
| -3000 | 44 | 11 | 20 | 21 | 27 |
| -2500 | 55 | 11 | 20 | 21 | 27 |

Table 3.14: The effect of increasing COVs on $\beta$ and number of exact buckling failure function evaluations for Approaches 2 and 6 at $N_x = -3000\ lb/in.$

| | COV=10% | | COV=20% | |
|---|---|---|---|---|
| | Approach 2 | Approach 6 | Approach 2 | Approach 6 |
| $\beta$ | 1.82 | 1.83 | 0.953 | 0.957 |
| $NFE^a$ | 33 | 25 | 33 | 25 |

[a] $NFE$ : number of exact buckling failure function evaluations

The values of basic random variables at the design point or MPP for $N_x = -3000\ lb/in.$ in Approaches 2 and 6 are compared in Table 3.15. Table 3.16 presents design point value for Approaches 2 and 6 for COVs of 10% and 20% for all random variables except ply orientation angles. The MPP values represent the worst combination of design properties resulting in buckling failure.

Table 3.15: Comparison of mean and MPP values for Approaches 2 and 6 at $N_x = -3000\ lb/in.$

| Random Variable | Mean Value | MPP Value | |
|---|---|---|---|
| | | Approach 2 | Approach 6 |
| $E_1, E+06\ psi$ | 18.0 | 17.68 | 17.58 |
| $E_2, E+06\ psi$ | 1.35 | 1.336 | 1.340 |
| $\nu_{12}$ | 0.226 | 0.22585 | 0.22586 |
| $G_{12}, E+06\ psi$ | 0.543 | 0.5389 | 0.5396 |
| $t_{\pm 45},\ in.$ | 0.04 | 0.0372 | 0.0371 |
| $t_{90},\ in.$ | 0.04 | 0.0375 | 0.0375 |
| $\theta_{\pm 45},\ deg.$ | 45 | 54.44 | 54.81 |
| $\theta_{90},\ deg.$ | 90 | 85.33 | 88.15 |
| $D, in.$ | 10 | 10.455 | 10.547 |
| $L, in.$ | 20 | 20.23 | 20.25 |

Table 3.16: The effect of increasing COVs on MPP values for the axial buckling in Approaches 2 and 6 at $N_x = -3000\ lb/in.$

| Random Variable (RV) | Mean Value | MPP Value | | | |
|---|---|---|---|---|---|
| | | $COV = 10\%$ | | $COV = 20\%$ | |
| | | Approach 2 | Approach 6 | Approach 2 | Approach 6 |
| $E_1, E+06\ psi$ | 18.0 | 16.70 | 16.57 | 16.54 | 16.48 |
| $E_2, E+06\ psi$ | 1.35 | 1.33 | 1.33 | 1.33 | 1.33 |
| $\nu_{12}$ | 0.226 | 0.22579 | 0.22580 | 0.22579 | 0.22579 |
| $G_{12}, E+06\ psi$ | 0.543 | 0.539 | 0.538 | 0.539 | 0.538 |
| $t_{\pm 45},\ in.$ | 0.04 | 0.0359 | 0.0359 | 0.0354 | 0.0357 |
| $t_{90},\ in.$ | 0.04 | 0.0365 | 0.0365 | 0.0361 | 0.0362 |
| $\theta_{\pm 45},\ deg.$ | 45 | 48.238 | 47.590 | 45.765 | 45.623 |
| $\theta_{90},\ deg.$ | 90 | 88.8188 | 89.6883 | 89.7881 | 89.9322 |
| $D, in.$ | 10 | 10.64 | 10.78 | 10.76 | 10.88 |
| $L, in.$ | 20 | 20.32 | 20.23 | 20.23 | 20.29 |

### 3.2.2 Sensitivity Analysis

The original and normalized probabilistic sensitivity derivatives for Approach 2 are shown in Table 3.17. Normalized probabilistic sensitivity derivatives of $\beta$ with respect to the mean and standard deviation of each random variable are shown in the Figure 3.6. Among all random variables affecting the axial buckling failure, cylinder diameter D is found to have the greatest influence, followed by elastic modulus $E_1$, and ply angles.

Table 3.17: Probabilistic sensitivity derivatives of $\beta$ for axial buckling in Approach 2 at $N_x = -3000\ lb/in.$

| RV | $\frac{\partial \beta}{\partial \mu_{X_i}}$ | $\delta_i$ | $\frac{\partial \beta}{\partial \sigma_{X_i}}$ | $\eta_i$ |
|---|---|---|---|---|
| $E_1$ | 3.16E-07 | 1.872 | -1.74E-07 | -0.0330 |
| $E_2$ | 1.42E-06 | 0.628 | -3.50E-07 | -0.0067 |
| $\nu_{12}$ | 0.3872 | 0.029 | -5.15E-03 | 0.0000 |
| $G_{12}$ | 1.72E-06 | 0.307 | -2.51E-07 | 0.0000 |
| $t_{\pm 45}$ | 230.0 | 0.378 | -321.17 | -0.0264 |
| $t_{90}$ | 206.0 | 0.339 | -258.15 | -0.0212 |
| $\theta_{\pm 45}$ | -0.1243 | -1.840 | -0.2347 | -0.3860 |
| $\theta_{90}$ | 0.0615 | 1.821 | -0.0574 | -0.0945 |
| $D$ | -0.5998 | -1.973 | -0.5462 | -0.0898 |
| $L$ | -0.0757 | -0.498 | -1.74E-02 | -0.0057 |

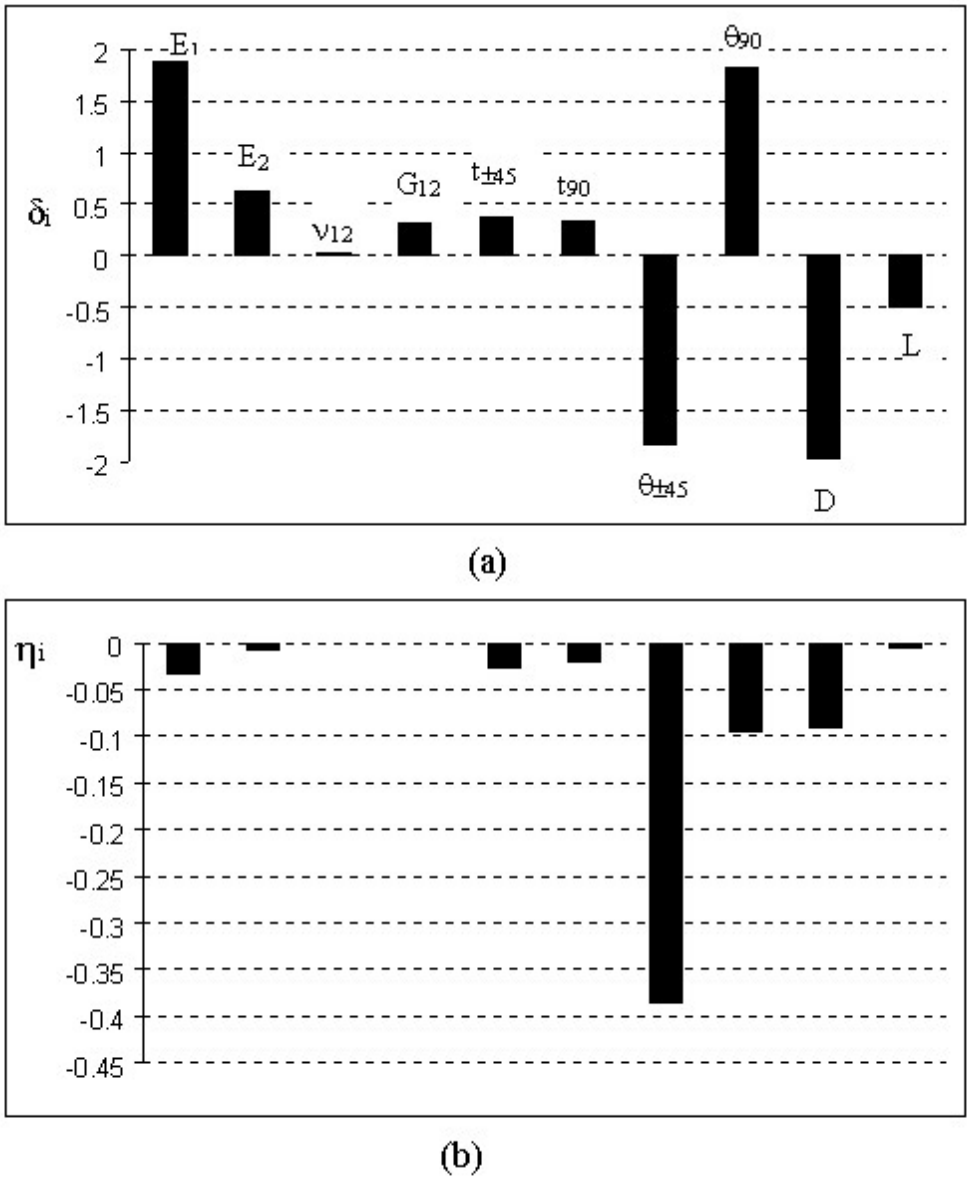


Figure 3.6: Normalized probabilistic sensitivity derivatives of $\beta$ for axial buckling load with respect to the (a) mean and (b) standard deviation of each random variable in Approach 2 at $N_x = -3000\ lb/in$.

The most important normalized probabilistic sensitivity derivatives, identified in Figure 3.6, obtained for Approaches 2-6 are presented in Table 3.18 and Figure 3.7 for comparison. The effect of increasing COVs on normalized probabilistic sensitivity derivatives are given in Table 3.19.

Table 3.18: Normalized probabilistic sensitivity derivatives $\delta_i$ for axial buckling in Approaches 2-6 at $N_x = -3000\ lb/in.$

| | Approach | | | | |
|---|---|---|---|---|---|
| RV | 2 | 3 | 4 | 5 | 6 |
| $E_1$ | 1.872 | 3.092 | 2.720 | 2.470 | 2.390 |
| $\theta_{\pm 45}$ | -1.840 | -1.608 | -1.419 | -1.888 | -1.850 |
| $\theta_{90}$ | 1.821 | -0.874 | 0.299 | 0.638 | 0.696 |
| $D$ | -1.973 | -2.604 | -2.959 | -2.374 | -2.294 |

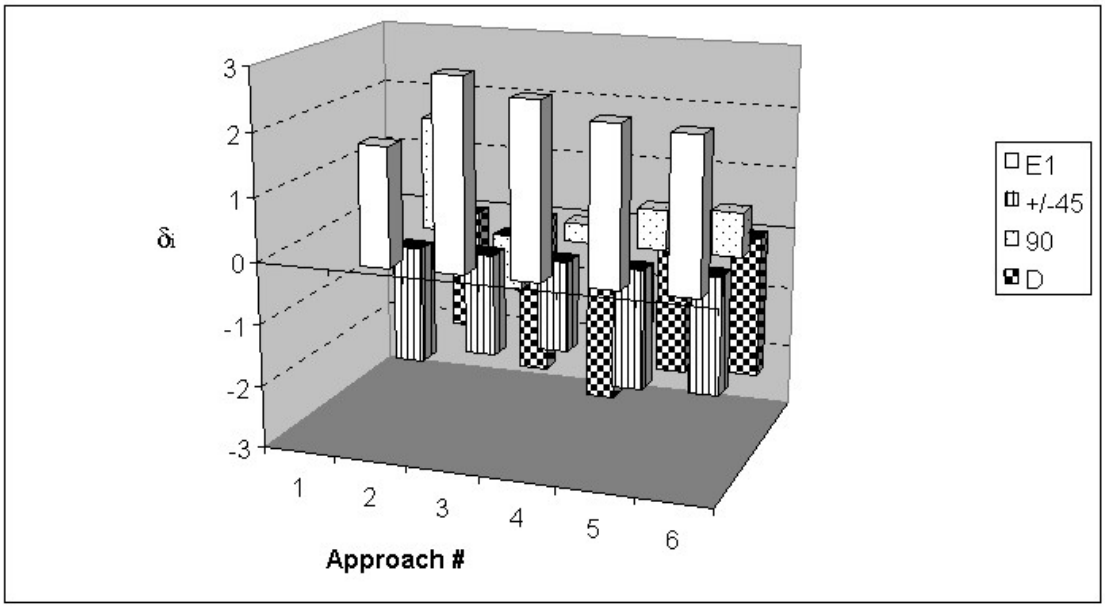


Figure 3.7: Comparison of $\delta_i$ for axial buckling load in Approaches 2-6 at $N_x = -3000\ lb/in.$

Table 3.19: The effect of increasing COVs on normalized probabilistic sensitivity derivatives for axial buckling load in Approaches 2 and 6 at $N_x = -3000\ lb/in.$

| | COV=10% | | | | COV=20% | | | |
|---|---|---|---|---|---|---|---|---|
| | Approach 2 | | Approach 6 | | Approach 2 | | Approach 6 | |
| RV | $\delta_i$ | $\eta_i$ | $\delta_i$ | $\eta_i$ | $\delta_i$ | $\eta_i$ | $\delta_i$ | $\eta_i$ |
| $E_1$ | 2.181 | -0.1575 | 2.375 | -0.1892 | 2.231 | -0.1809 | 2.314 | -0.1960 |
| $\theta_{\pm 45}$ | -1.761 | -0.1267 | -1.390 | -0.0800 | -1.516 | -0.0258 | -1.225 | -0.0170 |
| $\theta_{90}$ | 1.285 | -0.0169 | 0.335 | -0.0012 | 0.840 | -0.0020 | 0.267 | -0.0002 |
| $D$ | -1.929 | -0.1232 | -2.330 | -0.1821 | -2.084 | -0.1579 | -2.416 | -0.2137 |

# CHAPTER IV

# RELIABILITY-BASED STRUCTURAL OPTIMIZATION

The reliability-based structural optimization problem is formulated to find the optimal values of design variables $y_1, y_2, ..., y_{NDV}$ that would

$$\begin{aligned} &Minimize \quad f(\mathbf{X}) = c_1\mu_f(\mathbf{X}) + c_2\sigma_f(\mathbf{X}) \\ &subject\ to \qquad \beta_i^e \geq \beta_i^{e_{min}}, \qquad i = 1, 2, ..., NF \\ &\qquad\qquad {y_i}^l \leq y_i \leq {y_i}^u, \qquad i = 1, 2, ..., NDV \end{aligned} \tag{4.1}$$

where the objective function, $f(\mathbf{X})$ depends on the vector of random variables, $\mathbf{X}$ with $c_1$ and $c_2$ representing constant weight factors denoting the relative importance of the mean value and standard deviation of $f(\mathbf{X})$ in the optimization problem. Design constraints include limits on minimum reliability index associated with each failure mode denoted by $\beta_i^e$ and $NF$ is the number of uncorrelated failure modes. Design variables $y_1, y_2, ..., y_{NDV}$ represent the mean values of a subset of random variable vector $\mathbf{X}$ with specified lower and upper bounds.

The design optimization problem in equation (4.1) is applied to the composite cylinder described in Example 2, Chapter III such that $f$ is the cylinder weight given as

$$W = \pi \left[ \frac{(D + 2h)^2}{4} - \frac{D^2}{4} \right] L\ \rho \tag{4.2}$$

where $D$, $h$, and $L$ are the inner diameter, wall thickness, and length of cylinder, respectively. $\rho$ is the specific weight of the material, and is treated as a deterministic

parameter. Hence, the mean weight of cylinder is given as

$$\mu_f = \pi \left[ \frac{(\mu_D + 2\mu_h)^2}{4} - \frac{\mu_D^2}{4} \right] \mu_L \, \rho \tag{4.3}$$

where $\mu_D$, $\mu_h$, and $\mu_L$ are the mean diameter, mean thickness, and mean length of cylinder, respectively, and the standard deviation of weight is given as

$$\sigma_f = \sqrt{\left[ \left( \frac{\partial W}{\partial D} \right)^2 \sigma_D^2 + \left( \frac{\partial W}{\partial h} \right)^2 \sigma_h^2 + \left( \frac{\partial W}{\partial L} \right)^2 \sigma_L^2 \right]} \tag{4.4}$$

where $\sigma_D$, $\sigma_h$, and $\sigma_L$ are the standard deviation of diameter, thickness, and length of cylinder, respectively. Partial derivatives of weight with respect to the random variables are obtained by direct differentiation of equation (4.2), which gives

$$\begin{aligned} \frac{\partial W}{\partial D} &= \pi h L \, \rho \\ \frac{\partial W}{\partial h} &= \pi (D + 2h) L \, \rho \\ \frac{\partial W}{\partial L} &= \pi \left[ \frac{(D+2h)^2}{4} - \frac{D^2}{4} \right] \rho \end{aligned} \tag{4.5}$$

The cylinder is described to carry a uniform axial load in tension and compression. The failure of cylinder in tension is characterized by ply failure while that in compression is characterized by axial buckling. Minimum reliability index associated with each failure mode is denoted by $\beta_i^{e_{min}}$.

## 4.1 Optimization Solution

The optimization problem in equation (4.1) is solved using Su, et. al's [19] sequential local optimization technique (SLOT). In SLOT, the design space is divided into smaller subregions with the reliability index associated with each failure mode approximated using an RS model of corresponding limit-state function developed specifically for each subregion or local optimization. Upon completion of one local optimization cycle, a new

set of RS models is developed and the procedure is repeated until the solution converges to an optimum design point as shown in Figure 4.1, where S indicates the starting point in subregion 1 with the optimum design point shown as $\otimes$ in subregion 7.

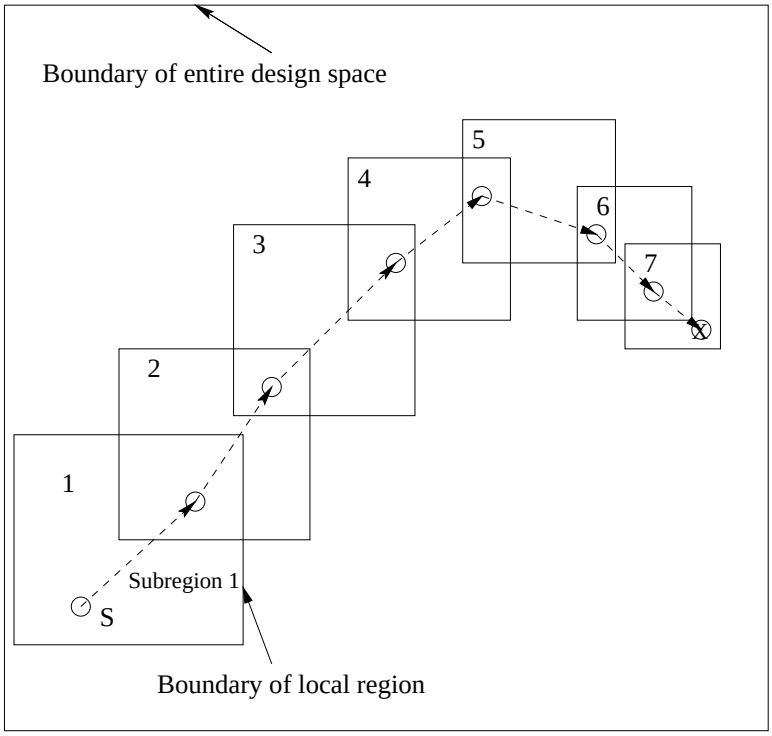


Figure 4.1: Illustration of sequential local optimization over multiple subregions

To perform the reliability-based structural optimization, the reliability analysis code developed here is coupled with the design optimization software DOT [25], and Approach 6, described previously in Chapter III, is used to calculate the reliability index for each failure mode. The optimization solution in each subregion is obtained using the method of sequential quadratic programming (SQP). Laminate configurations considered here include: $L1 : [\pm 45/90_4/\mp 45]_s$ and $L2 : [\pm 45/0_4/\mp 45]_s$, where fibers in $0^0$ plies are in axial direction and those in $90^0$ plies in the hoop direction. Both laminates have 16 plies, each made of carbon-epoxy (AS4 12k/3502) unidirectional tape with specific weight equal to 0.057 $lb/in^3$. Only the mean ply thicknesses are treated as design variables and allowed to change in each optimization cycle.

The flow chart describing the solution of reliability-based structural optimization problem is shown in Figure 4.2 with details in each numbered box described next.

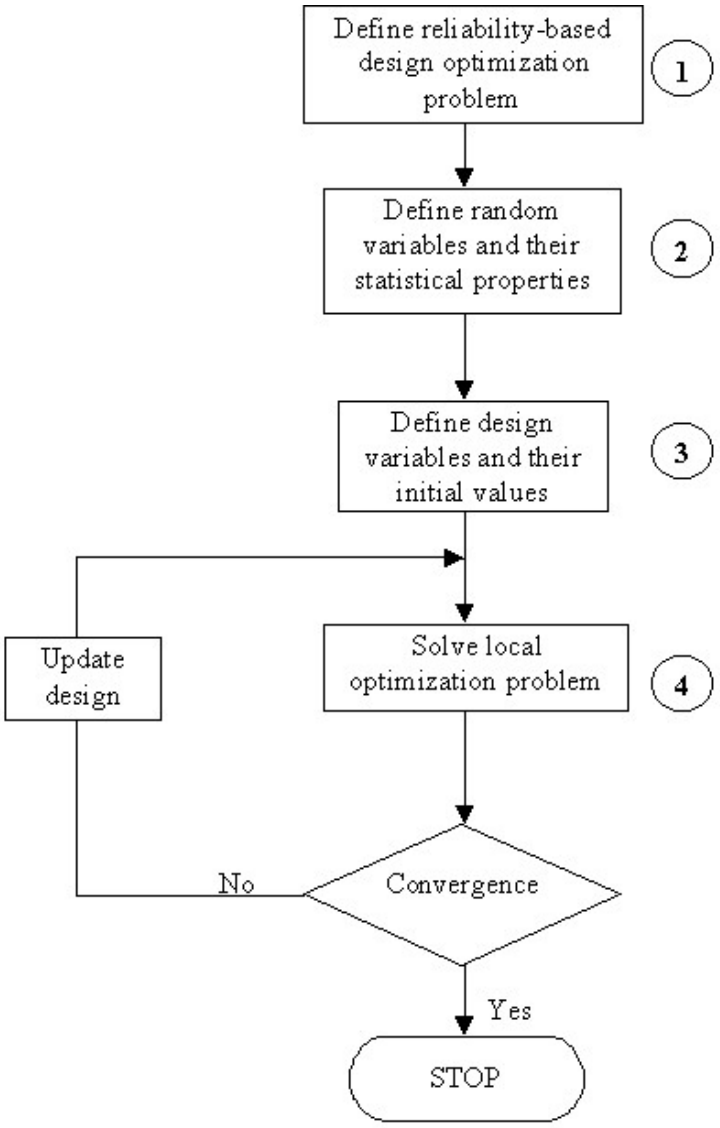


Figure 4.2: Solution procedure for the optimization problem

*Box 1*: The optimization problem is formulated as given by equation (4.1). Objective function $f(\mathbf{X})$ depends on the mean weight as well as the standard deviation of weight of the cylinder. In this case, weight factor $c_1 = 1$ and $c_2$ is calculated at the initial design point such that

$$c_2 = c_1 \frac{\mu_f(\mathbf{X})}{\sigma_f(\mathbf{X})} \tag{4.6}$$

where $\mu_f$ and $\sigma_f$ are obtained from equations (4.3) and (4.4), respectively. The values of $c_1$ and $c_2$ are kept fixed during the optimization process. For cylinders with $L1$ or $L2$ laminate configurations, there are three design constraints ($NF = 3$), two for ply failure and one for axial buckling.

*Box 2*: Of all random variables previously examined in the sensitivity analysis (see Example 1 & 2, Chapter III), only those with significant influence on ply failure (i.e., $F_2^t$, $\theta_{\pm 45}$, $E_2$, $E_1$ ) and axial buckling (i.e., $D$, $E_1$, $\theta_{\pm 45}$, $\theta_{90}$) are considered here. In addition, the thickness of each ply group as well as cylinder length are also treated as random. All random variables, as listed in Table 4.1, are assumed to have normal distribution with the specified mean values and coefficients of variation (COV).

Table 4.1: Statistical properties of random variables considered in the reliability-based design optimization problem

| Random Variable (RV) | Distribution Type | Mean Value | COV (%) |
|---|---|---|---|
| $E_1$ | Normal | 18.0e6 psi | 3.19 |
| $E_2$ | Normal | 1.35e6 psi | 4.26 |
| $F_2^t$ | Normal | 7.76e3 psi | 10.70 |
| $t_{ply}$ | Normal | $Y_i$ | 5.00 |
| $\theta_{ply}$ | Normal | $\pm 45^0$, $0^0$, $90^0$ | 5[a] |
| $D$ | Normal | 10 in. | 10.00 |
| $L$ | Normal | 10, 15, 20 in. | 10.00 |

[a]Standard Deviation

Hence, the 7 RVs affecting ply failure are: $E_1$, $E_2$, $F_2^t$, $t_{\pm 45}$, $t_{90}$ (or $t_0$), $\theta_{\pm 45}$, $\theta_{90}$ (or $\theta_0$), and the 7 RVs affecting axial buckling are: $E_1$, $t_{\pm 45}$, $t_{90}$ (or $t_0$), $\theta_{\pm 45}$, $\theta_{90}$ (or $\theta_0$), $D$, $L$

*Box 3*: For laminate configurations $L1$ and $L2$, there are only two design variables ($NDV = 2$), $t_{\pm 45}$ and $t_{90}$ (or $t_0$), where $t_{\pm 45}$ is the mean thickness of all $\pm 45^0$ plies and $t_{90}$ (or $t_0$) is the thickness of all $90^0$ (or $0^0$) plies in the laminate. The lower and upper bounds on design variables are chosen to be 0.016 *in.* and 0.064 *in.*, respectively. The side constraints imposed on design variables in each local optimization cycle are defined as

$$y_i^u, y_i^l = y_i^c \pm 3\sigma_{y_i} \tag{4.7}$$

where $y_i^c$ represents the initial value of thickness of the $i^{th}$ ply group at the beginning of each optimization cycle, and $\sigma_{y_i}$ is the corresponding standard deviation calculated as

$$\sigma_{y_i} = y_i^c \, (COV)_{y_i} \tag{4.8}$$

where $(COV)_{y_i}$ is the coefficient of variation of design variables. While $(COV)_{y_i}$ is kept fixed in the optimization analysis, $\sigma_{y_i}$ is allowed to change.

*Box 4*: The limit-state functions for ply failure and axial buckling are defined by equations (3.6) and (3.7), respectively, and shown here for convenience.

$$g^k = 1 - (f_1\sigma_1 + f_2\sigma_2 + f_{11}\sigma_1^2 + f_{22}\sigma_2^2 + f_{66}\tau_{12}^2 + 2f_{12}\sigma_1\sigma_2)_k \tag{3.6}$$

$$g = \frac{N_{cr}}{N_x} - 1 \tag{3.7}$$

At the beginning of each optimization cycle, failure functions are approximated by second-order RS models (equation (2.11)). Then, Gauss quadrature points, based on the number of random variables, are generated and used to perform target sampling of design space to generate $2n + 1$ response samples for use in calculating the regression coefficients. The statistical analysis software (SAS) is used for the regression analysis. The resulting second-order RS model for each failure function is used to calculate the corresponding $\beta$ using Approach 6 described previously in Chapter III.

The optimization problem in each subregion is solved using SQP method in DOT [25] for the applied load of 700 $lb/in$ in tension and $3,000$ $lb/in$ in compression. Minimum reliability index associated with each failure mode, i.e., $\beta_i^{e_{min}}$ is set equal to 3.72 in this analysis for an approximate reliability of 0.9999.

## 4.2 Optimization Results

The design optimization results for random variables defined in Table 4.1 are shown in column 3 of Table 4.2 below. Column 5 presents results for $COV = 10\%$ for all random variables except ply orientation angles that are kept at standard deviation $= 5^0$ as in Table 4.1. As the COVs (uncertainty) of the random variables are increased, the axial buckling load $N_{cr}$ increased by 9.8%, wall thickness $h$ $(= t_{\pm 45} + t_{90})$ by 4.5%, and objective function $f(\mathbf{X})$ by 4.6%. Reliability index associated with the $90^0$ layer $(\beta_{90})$ is an active constraint for small value of COV while that associated with the axial buckling $(\beta_b)$ becomes an active constraint at the large value of COV. Number of exact failure function evaluations for the corresponding reliability index is denoted by NFE.

Table 4.2: The effect of increasing COV on the cylinder optimization results for laminate $L1$, $\mu_D = 10$ $in.$, and $\mu_L = 20$ $in.$

| | COV=as in Table 4.1 | | COV=10% | |
|---|---|---|---|---|
| Parameter | Initial Design | Final Design | Initial Design | Final Design |
| $N_{cr}$, $lb/in$ | 4,282 | 5,778 | 4,282 | 6,342 |
| $f(\mathbf{X})$, $lb$ | 5.776 | 6.731 | 5.776 | 7.040 |
| $t_{\pm 45}$, $in$ | 0.04 | 0.0495 | 0.04 | 0.0550 |
| $t_{90}$, $in$ | 0.04 | 0.0437 | 0.04 | 0.0424 |
| $h$, $in$ | 0.08 | 0.0932 | 0.08 | 0.0974 |
| $\beta_{\pm 45}$ (NFE) | 4.60 | 6.39 (625) | 4.52 | 7.62 (1202) |
| $\beta_{90}$ (NFE) | 2.81 | **3.72 (222)** | 2.69 | 3.96 (310) |
| $\beta_b$ (NFE) | 2.76 | 5.11 (220) | 1.84 | **3.72 (299)** |
| CPU Time, hrs | | 27.8 | | 36.4 |

The convergence history for laminate $L1$ with $\mu_D = 10\ in.$ and $\mu_L = 20\ in.$ is shown in Figure 4.3. Convergence ($|f(\mathbf{X})_{m+1} - f(\mathbf{X})_m| \leq 0.01$, $m$ denotes iteration number) was reached after 4 optimization cycles. In general, 3 to 4 optimization cycles were needed to reach convergence. The reason for objective function increases between cycles 1 and 2 is the violation of two design constraints by the initial design as indicated by $\beta < 3.72$ in columns 2 and 4 of Table 4.2.

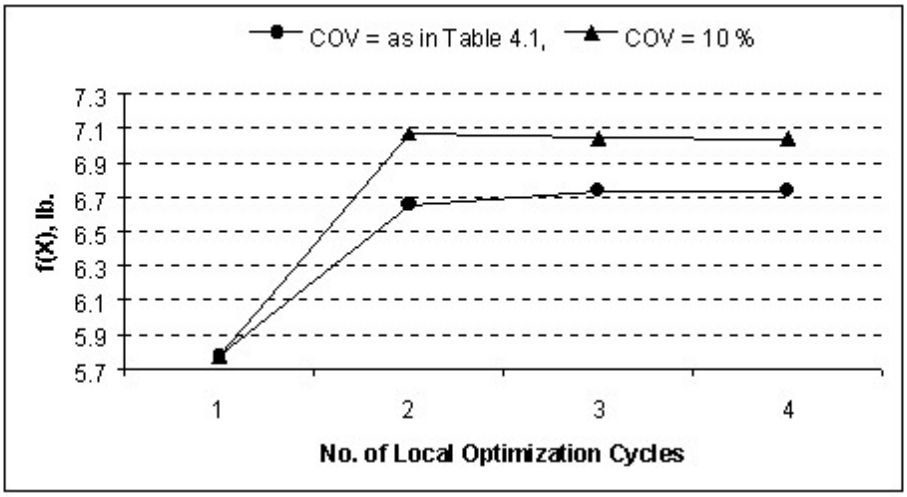


Figure 4.3: Convergence history for cylinder with laminate $L1$, $\mu_D = 10\ in.$, and $\mu_L = 20\ in.$

The effect of different geometrical properties and laminate configurations on optimization results is presented in Table 4.3. As the mean length of cylinder with laminate $L1$ increases, axial buckling load $N_{cr}$ decreases while wall thickness, $h$ and objective function, $f(\mathbf{X})$ both increase. Comparing results for laminates $L1$ and $L2$ for $\mu_L = 20\ in.$, cylinder with laminate $L1$ is found to be 20% stronger and 17.9% heavier. Reliability index associated with the $90^0$ layer ($\beta_{90}$) is an active constraint in cylinder with laminate $L1$ for all combinations of the diameter and length while $\beta_b$ is an active constraint in cylinder with laminate $L2$.

Table 4.3: Optimization results for cylinders with laminates $L1$ and $L2$ with $\mu_D = 10\ in.$

| Parameter | $L1$ | | | $L2$ |
|---|---|---|---|---|
| | $\mu_L = 10\ in.$ | $\mu_L = 15\ in.$ | $\mu_L = 20\ in.$ | $\mu_L = 20\ in.$ |
| $N_{cr},\ lb/in$ | 6,290 | 6,027 | 5,778 | 4,816 |
| $f(\mathbf{X}),\ lb$ | 3.345 | 5.021 | 6.731 | 5.710 |
| $t_{\pm 45},\ in$ | 0.0486 | 0.0489 | 0.0495 | 0.0449 |
| $t_{90}\ or\ t_0,\ in$ | 0.0439 | 0.0437 | 0.0437 | 0.0342 |
| $h,\ in$ | 0.0925 | 0.0926 | 0.0932 | 0.0791 |
| Active Constraint | $\beta_{90}$ | $\beta_{90}$ | $\beta_{90}$ | $\beta_b$ |
| CPU Time, hrs | 50.9 | 74.2 | 27.8 | 18.6 |

Computational (CPU) times shown in Tables 4.2 and 4.3 are recorded by solving the reliability-based structural optimization problem on a *Sun Ultra SPARC* computer with processor speed of 248 MHz . The total CPU time is found to also depend on the starting values chosen for the design variables.

# CHAPTER V

# SUMMARY AND CONCLUSIONS

In this thesis, the feasibility of Gauss quadrature points as means of target sampling of design space and generating accurate first- and second-order response surface models of failure functions was examined. Various alternative approaches for estimation of component reliability index were examined using two example problems: ply failure in a multidirectional composite laminate; and axial buckling of a composite circular cylinder. The effect of uncertainty in each random variable on reliability of each component was studied through the calculation of pertinent probabilistic sensitivity derivatives. As evident by the sensitivity analysis, the transverse tensile strength, ply orientation angles, and elastic moduli were the main contributors in the calculation of reliability index associated with Tsai-Wu ply failure criterion while cylinder diameter, elastic modulus in the fiber direction, and ply orientation angles were the main contributors in the calculation of reliability index for axial buckling failure. The computational efficiency and accuracy of various approaches were compared, and Approach 6 involving the use of exact limit-state function evaluation at each $\beta$ iteration and the use of second-order response surface model for calculation of partial derivatives was found to be the most efficient.

Approach 6 was applied in reliability-based design optimization of a composite circular cylinder with axial buckling and ply failure constraints. The optimization problem was solved by using sequential quadratic programming based on sequential local response surface approximations of limit-state functions for Tsai-Wu ply failure index and axial buckling load. The optimization solutions were presented for different coefficients

of variation, geometrical properties and laminate configurations. In the optimization problem, axial buckling load, ply thickness and cylinder weight were greatly influenced by the uncertainties in the selected random variables.

# APPENDIX A

# ALGORITHM TO CALCULATE RELIABILITY INDEX

The algorithm developed by Lee [21] is used to find the reliability index, $\beta$. The calculation of $\beta$ is achieved by performing the following computational steps:

1. Assume an initial value for the design point. It is common to start with the mean values of the basic random variables. The design point in the reduced coordinates is computed using

$$U_i = \frac{X_i - \mu_{X_i}}{\sigma_{X_i}} \qquad i = 1, 2, ..., n \tag{A.1}$$

2. Evaluate the directional cosines of the failure point. The partial derivatives needed to compute the directional cosines are obtained as

$$\left(\frac{\partial g}{\partial U_i}\right)_* = \left(\frac{\partial g}{\partial X_i}\right)_* \sigma_{X_i} \qquad i = 1, 2, ..., n \tag{A.2}$$

3. Find $\alpha_i^*$ using

$$\alpha_i^* = \frac{\left(\frac{\partial g}{\partial U_i}\right)_*}{\sqrt{\sum_{j=1}^{n}\left(\frac{\partial g}{\partial U_j}\right)_*^2}}, \qquad i = 1, 2, .., n \tag{A.3}$$

4. Calculate

$$\beta_{new} = \beta_{old} + \Delta\beta \tag{A.4}$$

where $\beta_{old} = 0$ for the first iteration, and $\Delta\beta$ is given as

$$\Delta\beta = \frac{g(\mathbf{X}^*)}{\sqrt{\sum_{j=1}^{n}\left(\frac{\partial g}{\partial U_j}\right)_*^2}} \tag{A.5}$$

5. Using the $\beta$ obtained from step 4, update the design point in $u$-space

$$u_{i_{new}}^* = -\alpha_i^* \beta_{new} \tag{A.6}$$

and then, update the design point in x-space

$$x_{i_{new}}^* = \mu_{X_i} + u_i^* \sigma_{X_i} \tag{A.7}$$

6. Repeat steps 1 to 5 until convergence is reached (i.e., $|g(\mathbf{X}^*)| \leq \epsilon, \epsilon = 0.001$).

The converged value of $\beta$ represents the shortest distance from the origin of the reduced coordinate system to the failure surface. The relationship between $\beta$ and the limit-state surface in the case of 2-dimensional problem is depicted in Figure A.1.

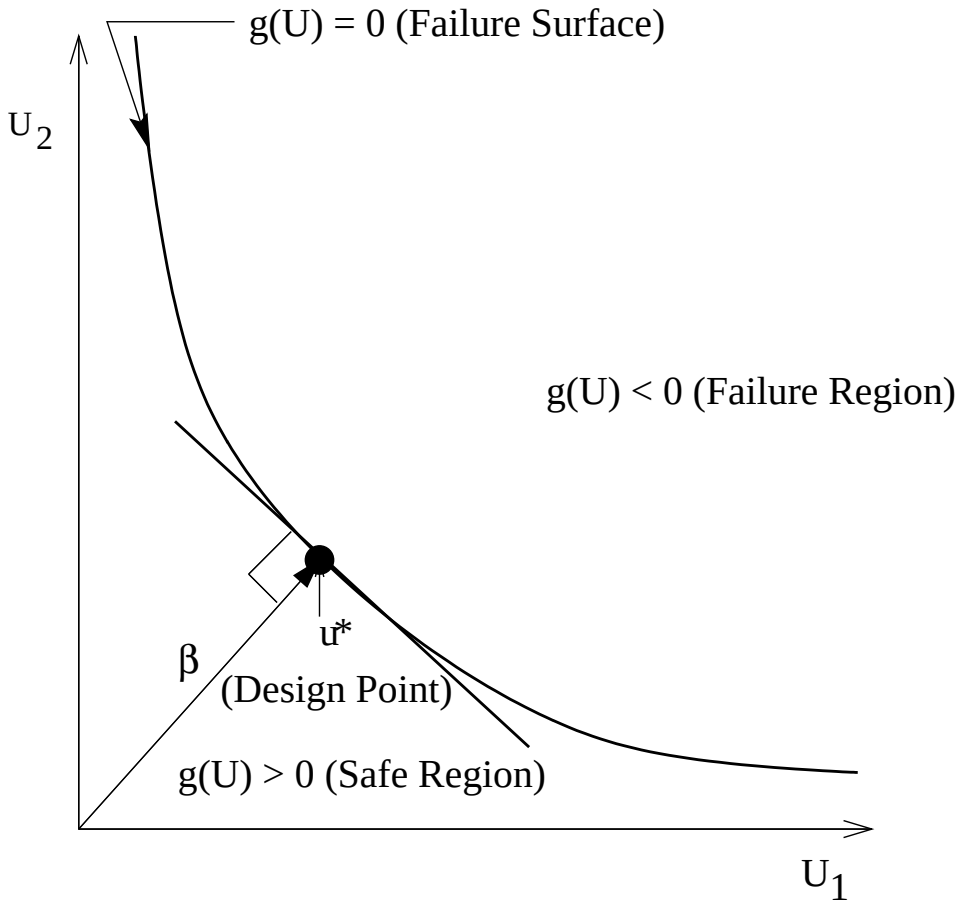


Figure A.1: Graphical representation of design point, failure surface and reliability index for 2-dimensional problem

This algorithm is deficient in calculating $\beta$ when random (independent) variables occur in the denominator of response surface model expression.

# APPENDIX B

# CALCULATION OF GAUSS QUADRATURE POINTS

Zhou and Nowak [22] developed integration formulas, developed originally by Stroud and Secrest [26], to compute the statistical parameters of a function of a random vector. The formula is a numerical procedure to estimate integrals using selected weights and points. The points and weights are predetermined in the independent standard normal variable space. The sample points in the basic variable space are obtained by special transformations. Various non-product integration formulas with $n+1$, $2n$, and $2n^2+1$ simulation cycles ($n$ is the number of random variables) have been developed. Numerical problems with single variable function, multivariate function and modeling of reinforced concrete section have been solved using the various point integration technique presented in the paper and results are compared with Monte Carlo simulations. It has been observed that point integration formulas give results with good accuracy in very less computational time. The technique presented allows for a direct use of the available deterministic computer programs, and is very easy to implement.

For a linear RS model involving $n+1$ unknown coefficients, the procedure relies on the use to $n+1$ quadrature model. The values of $j^{th}$ random variable for $i^{th}$ sampling experiment is defined according to the equation

$$x_{i,j} = \mu_{X_j} + Z_{i,j}\sigma_{X_j} \quad i = 1, 2, ..., m \quad j = 1, 2, ..., n \tag{B.1}$$

where $\mu_{X_j}$ and $\sigma_{X_j}$ are the mean and standard deviation of random variable $X_j$.

For $m = n + 1$, the Gauss quadrature points, $Z_{i,j}$ are determined as

$$\begin{aligned}
Z_{1,j} &= (\sqrt{n}, 0, 0, ..., 0) \\
Z_{2,j} &= \left(-\sqrt{\tfrac{1}{n}}, \sqrt{\tfrac{(n+1)(n-1)}{n}}, 0, ..., 0\right) \\
Z_{3,j} &= \left(-\sqrt{\tfrac{1}{n}}, -\sqrt{\tfrac{(n+1)}{n(n-1)}}, \sqrt{\tfrac{(n+1)(n-2)}{(n-1)}}, 0, ..., 0\right) \\
Z_{4,j} &= \left(-\sqrt{\tfrac{1}{n}}, -\sqrt{\tfrac{n+1}{n(n-1)}}, -\sqrt{\tfrac{(n+1)}{(n-1)(n-2)}}, \sqrt{\tfrac{(n+1)(n-3)}{(n-2)}}, 0, ..., 0\right) \\
&\vdots \\
Z_{n,j} &= \left(-\sqrt{\tfrac{1}{n}}, -\sqrt{\tfrac{(n+1)}{n(n-1)}}, -\sqrt{\tfrac{(n+1)}{(n-1)(n-2)}}, -\sqrt{\tfrac{(n+1)}{(n-2)(n-3)}}, ..., \sqrt{\tfrac{n+1}{2}}\right) \\
Z_{n+1,j} &= \left(-\sqrt{\tfrac{1}{n}}, -\sqrt{\tfrac{(n+1)}{n(n-1)}}, -\sqrt{\tfrac{(n+1)}{(n-1)(n-2)}}, -\sqrt{\tfrac{(n+1)}{(n-2)(n-3)}}, ..., -\sqrt{\tfrac{n+1}{2}}\right)
\end{aligned} \tag{B.2}$$

Hence, in the first simulation all random variables are kept at their respective mean values except the first random variable, which is perturbed as

$$x_1 = \mu_{X_1} + \sqrt{n}\sigma_{X_1} \tag{B.3}$$

The graphical representation of how the random variables are obtained for the first, second, $n^{th}$ and $(n+1)^{th}$ simulations are given in Figure B.1.

For $m = 2n$, the Gauss quadrature points, $Z_{i,j}$ are defined as [22]

$$\begin{aligned}
Z_{1,j} &= -Z_{n+1,j} = (\sqrt{n}, 0, 0, ..., 0, 0) \\
Z_{2,j} &= -Z_{n+2,j} = (0, \sqrt{n}, 0, ..., 0, 0) \\
Z_{3,j} &= -Z_{n+3,j} = (0, 0, \sqrt{n}, ..., 0, 0) \\
&\vdots \\
Z_{n,j} &= -Z_{n+n,j} = (0, 0, 0, ..., 0, \sqrt{n})
\end{aligned} \tag{B.4}$$

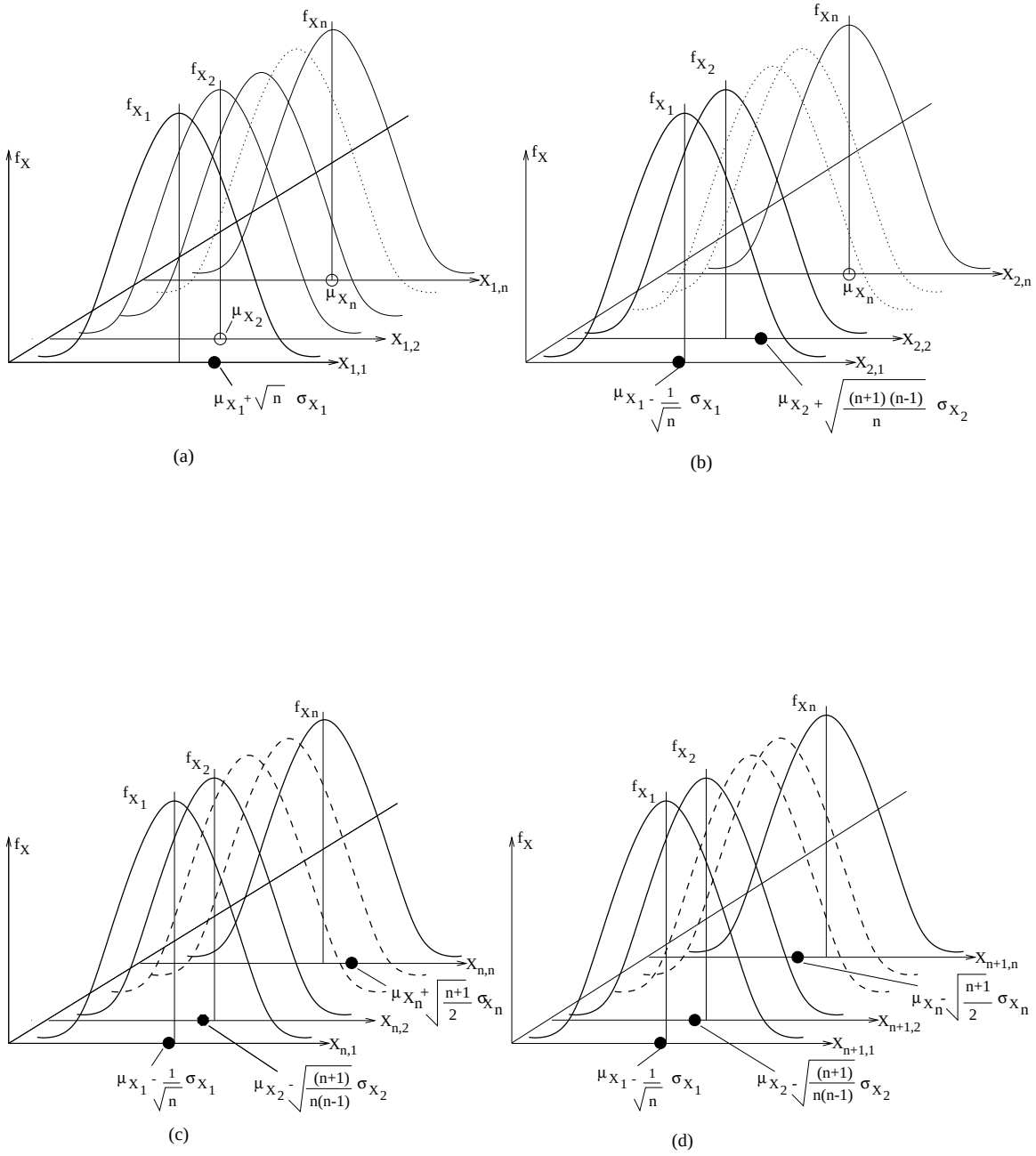


Figure B.1: Depiction of random values selected for the (a) first (b) second (c) $n^{th}$ and (d) $(n+1)^{th}$ simulations

# APPENDIX C

# IN-PLANE STRESSES IN PRINCIPAL MATERIAL DIRECTIONS

The in-plane stresses in PMD in $k^{th}$ layer are given as [27]

$$\{\sigma\}_k = [T]_k \left[\bar{Q}\right]_k [A]^{-1}\{N\} \tag{C.1}$$

$\Rightarrow$

$$\begin{Bmatrix} \sigma_1 \\ \sigma_2 \\ \tau_{12} \end{Bmatrix}_k = \begin{bmatrix} m^2 & n^2 & 2mn \\ n^2 & m^2 & -2mn \\ -mn & mn & m^2-n^2 \end{bmatrix}_k \begin{bmatrix} \bar{Q}_{11} & \bar{Q}_{12} & \bar{Q}_{16} \\ \bar{Q}_{12} & \bar{Q}_{22} & \bar{Q}_{26} \\ \bar{Q}_{16} & \bar{Q}_{26} & \bar{Q}_{66} \end{bmatrix}_k \begin{bmatrix} A_{11} & A_{12} & A_{16} \\ A_{12} & A_{22} & A_{26} \\ A_{16} & A_{26} & A_{66} \end{bmatrix}^{-1} \begin{Bmatrix} N_x \\ N_y \\ N_{xy} \end{Bmatrix} \tag{C.2}$$

calculate $\left[\bar{Q}\right]$ for $k^{th}$ layer as

$m = cos(\theta) \qquad n = sin(\theta)$

$$\begin{aligned} \bar{Q}_{11} &= U_1 + U_2\, cos(2\theta) + U_3\, cos(4\theta) \\ \bar{Q}_{12} &= U_4 - U_3\, cos(4\theta) \\ \bar{Q}_{16} &= \tfrac{U_2}{2}\, sin(2\theta) + U_3\, sin(4\theta) \\ \bar{Q}_{22} &= U_1 - U_2\, cos(2\theta) + U_3\, cos(4\theta) \\ \bar{Q}_{26} &= \tfrac{U_2}{2}\, sin(2\theta) - U_3\, sin(4\theta) \\ \bar{Q}_{66} &= \tfrac{1}{2}(U_1 - U_4) - U_3\, cos(4\theta) \end{aligned} \tag{C.3}$$

where

$$\begin{aligned} U_1 &= \tfrac{1}{8}(3Q_{11} + 3Q_{22} + 2Q_{12} + 4Q_{66}) \\ U_2 &= \tfrac{1}{2}(Q_{11} - Q_{22}) \\ U_3 &= \tfrac{1}{8}(Q_{11} + Q_{22} - 2Q_{12} - 4Q_{66}) \\ U_4 &= \tfrac{1}{8}(Q_{11} + Q_{22} + 6Q_{12} - 4Q_{66}) \end{aligned} \tag{C.4}$$

where

$$\begin{aligned} Q_{11} &= \tfrac{E_1}{1-\nu_{12}\nu_{21}}; \quad & Q_{12} &= \tfrac{\nu_{12}E_2}{1-\nu_{12}\nu_{21}} \\ Q_{22} &= \tfrac{E_2}{1-\nu_{12}\nu_{21}}; \quad & Q_{66} &= G_{12} \\ \nu_{21} &= \tfrac{E_2}{E_1}\nu_{12} \end{aligned} \tag{C.5}$$

and

$$A_{ij} = \sum_{k=1}^{N_L} (\bar{Q}_{ij})_k t_k \tag{C.6}$$

where $i = 1, 2$ and $j = 1, 2, 6$

$N_L$ is the total number of layers and $t_k$ is the thickness of each layer in a composite laminate.

# APPENDIX D

# BUCKLING ANALYSIS OF COMPOSITE SHELL

The cylindrical shells considered in this work fall under the category of thin shell structures ($R/t > 20$) with the displacement field described according to a first-order shear deformation theory (FSDT) given as

$$\begin{aligned} u(x,y,z) &= u_0(x,y) + z\phi_x(x,y) \\ v(x,y,z) &= v_0(x,y) + z\phi_y(x,y) \\ w(x,y,z) &= w_0(x,y) \end{aligned} \tag{D.1}$$

where $u_0, v_0, w_0$ are the mid-plane (membrane) displacement in the $x, y, z$ directions, respectively, and $\phi_x, \phi_y$ are the cross-sectional rotations about the $y$ and $x$ axes, respectively. The axial coordinate is $x$, the circumferential coordinate is $y$, and the thickness coordinate normal to the shell surface is $z$ as shown in Figure 3.4. According to FSDT, cross-sections normal to the reference plane before deformation are assumed to remain planar but not necessarily normal to the mid-surface after deformation. The linear strain-displacement relations are based on Sanders-Koiter shell theory, can be given as [24]

$$\begin{aligned} \epsilon_{xL} &= \epsilon_x^0 + z\kappa_x \\ \epsilon_{yL} &= \epsilon_y^0 + z\kappa_y \\ \gamma_{xyL} &= \gamma_{xy}^0 + z\kappa_{xy} \\ \gamma_{xzL} &= \gamma_{xz}^0 \\ \gamma_{yzL} &= \gamma_{yz}^0 \end{aligned} \tag{D.2}$$

where the in-plane strains ($\epsilon_x^0, \epsilon_y^0, \gamma_{xy}^0$, at $z = 0$), transverse shear strains ($\gamma_{xz}^0, \gamma_{yz}^0$, at $z = 0$), and curvatures ($\kappa_x, \kappa_y, \kappa_{xy}$) are given by

$$\begin{aligned}
\epsilon_x^0 &= \frac{\partial u_0}{\partial x} \\
\epsilon_y^0 &= \frac{\partial v_0}{\partial y} + \frac{\partial w_0}{R} \\
\gamma_{xy}^0 &= \frac{\partial u_0}{\partial y} + \frac{\partial v_0}{\partial x} \\
\kappa_x &= \frac{\partial \phi_x}{\partial x} \\
\kappa_y &= \frac{\partial \phi_y}{\partial y} \\
\kappa_{xy} &= \frac{\partial \phi_x}{\partial y} + \frac{\partial \phi_y}{\partial x} + \frac{1}{2R}\left(-\frac{\partial u_0}{\partial y} + \frac{\partial v_0}{\partial x}\right) \\
\gamma_{xz}^0 &= \phi_x + \frac{\partial w_0}{\partial x} \\
\gamma_{yz}^0 &= \phi_y + \frac{\partial w_0}{\partial y} - \frac{v_0}{R}
\end{aligned} \tag{D.3}$$

where R is the radius of the cylindrical shell.

The critical buckling stress is determined on the basis of the principal that during the buckling the elastic strain energy stored in the structure is equal to the work done by the applied load. The elastic strain energy (U) for a composite cylindrical shell is

$$U = \frac{1}{2}\int_A \{\epsilon\}^T \begin{bmatrix} A_{ij} & B_{ij} & 0 \\ B_{ij} & D_{ij} & 0 \\ 0 & 0 & C_{pq} \end{bmatrix} \{\epsilon\} dA \tag{D.4}$$

where

$$\{\epsilon\}^T = \left\{ \begin{array}{cccccccc} \epsilon_x^0 & \epsilon_y^0 & \gamma_{xy}^0 & \kappa_x & \kappa_y & \kappa_{xy} & \gamma_{xz}^0 & \gamma_{yz}^0 \end{array} \right\}^T \tag{D.5}$$

and is given by equation (D.3). $A_{ij}, B_{ij}, D_{ij}$ are the laminate extensional, coupling, bending stiffness matrices, respectively and $C_{pq}$ is the transverse shear stiffness coefficient.

Considering a linear buckling analysis with a prescribed uniform in-plane prestress state, the work done (W) by the applied edge load is given as

$$W = \frac{1}{2}\int_A \overline{N}_x \left[\left(\frac{\partial v_0}{\partial x}\right)^2 + \left(\frac{\partial w_0}{\partial x}\right)^2\right] dA \tag{D.6}$$

where $\overline{N}_x$ is the stress resultant in the x direction.

To calculate the axial buckling load, the displacements $u_0, v_0, w_0$ and rotations $\phi_x, \phi_y$ are approximated by different Ritz functions with Legendre polynomials used as the interpolation functions such that the essential boundary conditions are satisfied. Then by applying the principal of minimum total potential energy, the critical load is obtained by setting equations (D.4) and (D.6) equal to each other and solving the resultant eigenvalue problem, by using an eigenvalue solver (e.g., power iteration, QR-iteration), for the critical buckling load factor $\lambda_{cr}$ such that

$$N_{cr} = \lambda_{cr} N_x \tag{D.7}$$

A computer implementation [24] of the described mathematical procedure is used to calculate the axial buckling load of the anisotropic circular cylindrical shells with clamped loaded edges. This code is preferred to use because of the simplicity in modeling the circular cylindrical shells. In this code, the circular cylindrical shell is modeled as a semi-circular shell with symmetric boundary conditions along the two unloaded edges 1 and 3. In defining the boundary conditions, edge shortening is allowed along edge 4 with edge 2 kept fixed. The conditions of symmetry require the $v$ displacement and $\phi_y$ rotation to be kept zero along edges 1 and 3 (Figure 3.4).

## REFERENCES


[1] T. Y. Torng, H.-Z. Lin, and M. R. Khalessi, "Reliability calculation based on a robust importance sampling method," in *Proceedings of the 37'th AIAA/ASME/ASCE/AHS/ASC Structures, Structural Dynamics, and Materials Conference*, pp. 1316–1325, Part 3, Salt Lake City, UT, April 15–17, 1996.

[2] C. G. Bucher, "Adaptive sampling in an iterative fast Monte Carlo procedure," *Structural Safety*, vol. 5, no. 2, pp. 119–126, June 1988.

[3] Y.-T. Wu, "Computational methods for efficient structural reliability and reliability sensitivity analysis," *AIAA Journal*, vol. 32, no. 8, pp. 1717–1723, 1994.

[4] A. M. Hasofer and N. Lind, "An exact and invariant first-order reliability format," *Journal of Engineering Mechanics*, vol. 100, no. EM1, pp. 111–121, 1974.

[5] R. Rackwitz and B. Fiessler, "Structural reliability under combined random load sequences," *Computers and Structures*, vol. 9, pp. 489–494, 1978.

[6] M. Miki, Y. Murotsu, T. Tanaka, and S. Shao, "Reliability of unidirectional fibrous composites," *AIAA Journal*, vol. 28, no. 11, pp. 1980–1986, 1990.

[7] C. G. Bucher and U. Bourgund, "A fast and efficient response surface approach for structural reliability problems," *Structural Safety*, vol. 7, no. 1, pp. 57–66, 1990.

[8] Y. W. Liu and F. Moses, "A sequential response surface method and its application in the reliability analysis of aircraft structural systems," *Structural Safety*, vol. 16, no. 10, pp. 39–46, 1994.

[9] H. R. Millwater and Y.-T. Wu, "Global/local methods for probabilistic structural analysis," in *Proceedings of the 34'th AIAA/ASME/ASCE/AHS/ASC Structures, Structural Dynamics, and Materials Conference*, pp. 701–706, La Jolla, CA, April 19-22, 1993.

[10] S. Shao and Y. Murotsu, "Structural reliability analysis using a neural network," *A Hen/Transactions of the Japan Society of Mechanical Engineers*, vol. 62, no. 603, pp. 2628–2634, 1996.

[11] M. Rais-Rohani and M. N. Singh, "Efficient response surface approach for reliability estimation of composite structures," in *Proceedings of the 9'th AIAA/ISSMO Symposium on Multidisciplinary Analysis and Optimization*, Atlanta, GA, September 4–6, Paper No. AIAA-2002-5604, 2002.

[12] L. D. Liaw and R. I. DeVries, "Reliability-based optimization for robust design," *International Journal of Vehicle Design*, vol. 25, nos. 1/2, pp. 64–77, 2001.

[13] L. Wang, R. V. Grandhi, and D. A. Hopkins, "Structural reliability optimization using an efficient safety index calculation procedure," *International Journal for Numerical Methods in Engineering*, vol. 38, no. 10, pp. 1721–1738, May 1995.

[14] T. Y. Torng and R. J. Yang, "An advanced reliability-based optimization method for structural system design," in *Proceedings of the 34'th AIAA/ASME/ASCE/AHS/ASC Structures, Structural Dynamics, and Materials Conference*, pp. 1198–1206, La Jolla, CA, April 19–22, 1993.

[15] S. Hendawi and D. M. Frangopol, "Design of composite hybrid plate girder bridges based on reliability and optimization," *Structural Safety*, vol. 15, no. 1–2, pp. 149–165, August 1994.

[16] L. Yang and Z. K. Ma, "Optimum design based on reliability for a composite structural system," *Computers and Structures*, vol. 36, no. 5, pp. 785–790, 1990.

[17] E. Nikolaidis and R. Burdisso, "Reliability based optimization: a safety index approach," *Computers and Structures*, vol. 28, no. 6, pp. 781–788, 1988.

[18] J. Tu, K. K. Choi, and Y. H. Park, "A new study on reliability-based design optimization," *Journal of Mechanical Design*, vol. 121, no. 4, pp. 557–564, December 1999.

[19] B. Su, M. Rais-Rohani, and M. N. Singh, "Reliability-based optimization of anisotropic cylindrical shells with response surface approximations of buckling instability," in *Proceedings of the 43'rd AIAA/ASME/ASCE/AHS/ASC Structures, Structural Dynamics, and Materials Conference*, Denver, CO, April 22–25, Paper No. AIAA-2002-1386, 2002.

[20] D. B. Bryan and D. Nolan, *Reliabiltiy Engineering Handbook*. Quality Publishing, 1999.

[21] Y.-H. Lee, *Stochastic Finite Element Analysis of Structural Plain Concrete*. PhD thesis, Department of Civil, Environmental and Architectural Engineering, University of Colordo, Boulder, CO., 1994.

[22] J.-H. Zhou and A. Nowak, "Integration formulas to evaluate functions of random variables," *Structural Safety*, vol. 5, pp. 267–284, 1988.

[23] Materials Sciences Corporation; University of Delaware; Army Research Laboratory, *The Composite Materials Handbook, MIL-17*, http://www.mil17.org.

[24] N. Jaunky and N. Knight, "An assessment of shell theories for buckling of cylindrical shells," *International Journal of Solids and Structures*, vol. 36, pp. 3799–3820, 1999.

[25] Vanderplaats Research and Development Inc., *DOT-Design Optimization Tools*, 1999.

[26] A. H. Stroud and D. Secrest, "Approximate integration formulas for certain spherically symmetric regions," *Mathematics of Computation*, vol. 17, pp. 105–135, 1963.

[27] I. M. Daniel and O. Ishai, *Engineering Mechanics of Composite Materials*. Oxford University Press, Inc., 1994.